

Comparison between geodetic and oceanographic approaches to estimate mean dynamic topography for vertical datum unification: evaluation at Australian tide gauges

M.S. Filmer¹, C.W. Hughes^{2,3}, P.L. Woodworth³, W.E. Featherstone¹, R.J. Bingham⁴

¹School of Earth and Planetary Sciences & The Institute for Geoscience Research, Curtin University, GPO Box U1987, Perth WA 6845, Australia

²School of Environmental Sciences, University of Liverpool, Liverpool L69 3GP, United Kingdom

³National Oceanography Centre, Joseph Proudman Building, 6 Brownlow Street, Liverpool L3 5DA, United Kingdom

⁴School of Geographical Sciences, Bristol Glaciology Centre, University of Bristol, Bristol BS8 1TH, United Kingdom

Corresponding author: Mick Filmer M.Filmer@curtin.edu.au

ORCID: M.S. Filmer (0000-0002-3555-4869), C.W. Hughes (0000-0002-9355-0233), P.L. Woodworth (0000-0002-6681-239X), W.E. Featherstone (0000-0001-9644-4535), R.J. Bingham (0000-0003-0609-5672)

Abstract

The direct method of vertical datum unification requires estimates of the ocean's mean dynamic topography (MDT) at tide gauges, which can be sourced from either geodetic or oceanographic approaches. To assess the suitability of different types of MDT for this purpose, we evaluate 13 physics-based numerical ocean models and six MDTs computed from observed geodetic and/or ocean data at 32 tide gauges around the Australian coast. We focus on the viability of numerical ocean models for vertical datum unification, classifying the 13 ocean models used as either independent (do not contain assimilated geodetic data) or non-independent (do contain assimilated geodetic data). We find that the independent and non-independent ocean models deliver similar results. Maximum differences among ocean models and geodetic MDTs reach >150 mm at several Australian tide gauges, and are considered anomalous at the 99% confidence level. These differences appear to be of geodetic origin, but without additional independent information, or formal error estimates for each model, some of these errors remain inseparable. Our results imply that some ocean models have standard deviations of differences with other MDTs (using geodetic and/or ocean observations) at Australian tide gauges, and with levelling between some Australian tide gauges, of $\sim \pm 50$ mm. This indicates that they should be considered as an alternative to geodetic MDTs for the direct unification of vertical datums. They can also be used as diagnostics for errors in geodetic MDT in coastal zones, but the inseparability problem remains, where the error cannot be discriminated between the geoid model or altimeter-derived mean sea surface.

Keywords: mean dynamic topography, vertical datum unification, mean sea surface, geoid, numerical ocean models.

1 Introduction

The ocean's time-mean dynamic topography (MDT) is the difference between the time-mean sea surface (MSS) and the geoid. In the geodetic literature, it is also referred to as sea surface topography or dynamic ocean topography. Knowledge of the MDT is of interest to oceanographers to study the ocean's surface currents (e.g., Wunsch 1978; Wunsch and Gaposchkin 1980; Ganachaud et al. 1997; Marshall et al. 1997a, 1997b; Wunsch and Stammer 1998), and to geodesists to unify or

analyse height datums globally (e.g., Rummel and Ilk 1995; Rummel 2001; Woodworth et al. 2012) or locally (e.g., Featherstone and Filmer 2012; Bolkas et al. 2012; Filmer and Featherstone 2012; Penna et al. 2013).

Many national vertical datums (referred to herein as local vertical datums; LVDs) have been realised by constraining national levelling networks to a zero height at mean sea level (MSL; as an approximation of the geoid) at single or multiple tide gauges (e.g., Roelse et al. 1971; Zilkoski et al. 1992; Christie 1994). This introduces offsets of up to 1 m in magnitude from the W_0 geoid (e.g., Rapp 1994) due to the spatially varying MDT. Unification of LVDs has been discussed over decades in the geodetic literature (e.g., Colombo 1980; Rummel and Teunissen 1988; Rapp and Balasubramania 1992; Xu 1992; Balasubramania 1994; among many others), but a solution has so far been restricted by the lack of adequate data.

Rummel (2001) sets out three methods for LVD unification: (1) geodetic levelling among LVDs within one landmass, (2) oceanographic levelling (steric, dynamic or altimetric) connecting tide gauges, and (3) the geodetic boundary value approach. Methods (1) and (2) are classified as direct methods, with (3) indirect. Progress using the indirect method (3) has been made due to improved global gravitational models (GGMs) (e.g., Arabelos and Tscherning 2001; Ardalan and Safari 2005; Amos and Featherstone 2009; Zhang et al. 2009; Gruber et al. 2012; Gerlach and Rummel 2013; Amjadiparvar et al. 2016; Sánchez et al. 2016; Grombein et al. 2017, and many others), facilitated most recently by data from the Gravity Recovery and Climate Experiment (GRACE, Tapley et al. 2004) and the Gravity field and steady-state Ocean Circulation Explorer (GOCE; Drinkwater et al. 2003). A limitation with method (3) is that gravimetric geoid models are problematic in coastal regions, primarily due to insufficient gravity data along the coastal boundary (e.g., Hipkin 2000; Amjadiparvar et al. 2016) and omission errors due to the limited spatial resolution of the geoid model (e.g., Losch et al. 2002; Vossepoel 2007; Bingham et al. 2008; Gruber et al. 2012; Mazloff et al. 2014). This is exacerbated by satellite altimeter-derived gravity anomalies used in geoid models containing larger uncertainties in the coastal zone than in the deep ocean, because of land contamination of altimeter and radiometer footprints and greater uncertainties in tidal, atmospheric and other corrections (e.g., Andersen 1999; Deng et al. 2002; Volkov et al. 2007; Andersen et al. 2010; Vignudelli et al. 2011; Claessens 2012; Slobbe and Klees 2014).

Direct method (1) is not possible for LVDs separated by ocean, which leads our interest to method (2), though using the single vertical datum over the continent of Australia permits us to compare methods (1) and (2) in Section 5. An accurate estimate of MDT at the respective LVD's tide gauges can directly determine the LVD offsets at their datum origin. The MDT can be sourced from geodetic methods (referred to as altimetric by Rummel (2001)), oceanographic methods, or their combination (see Section 2.1 for their classification). The possibility that physics-based oceanographic models may provide a superior data source to method (3) for vertical datum unification (cf. Woodworth et al. 2012; Bolkas et al. 2012), is the main focus of this study.

We discuss the construction and classification of a number of MDT models derived using different sets of data (tide gauge MSL, satellite altimetry, ocean models and geoid models), in order to test which may be the most suitable for vertical datum unification (VDU) using method (2). The lack of formal errors for all MDTs impedes a definitive identification of the suitability of each one for unifying LVDs. This led us to make inferences from a combination of independent or quasi-independent MDTs to provide insight into the possible errors associated with coastal MDT estimates. The reason for using a large range of MDTs is to provide sufficient independence and redundancy to allow robust inference from these comparisons.

The Australian continent is used as a test platform for comparison of different MDTs because of its long (~60,000 km) coastline that includes a range of different conditions, including broad continental shelves, a western boundary current adjacent to a narrow, steep continental shelf, embayments that are almost isolated from the open ocean, tropical to mid-latitude conditions, and exposure to both subtropical and subpolar oceans. It also provides 32 tide gauges with co-located

GNSS observations, all of which are used so as to provide redundancy and testing in the different conditions, and avoid subjectively selecting sites in advance that may produce more favourable results, i.e., the study includes robust ocean model comparisons that are conducted in challenging areas. We acknowledge that the results of the study are unique to Australia, but suggest that using 32 tide gauges over a large area of the Southern Hemisphere (latitude -10° to -43° ; longitude 115° to 154°) provides a range of conditions (described above) that may be encountered elsewhere around the world.

2 Data and methods

The following subsections introduce the MDT data and methods used. Table 1 summarises this MDT information, grouped according to the classifications (a) through (e) in Section 2.1. A discussion on possible errors is in Section 2.6. We compare datasets averaged over the five-year period 2003-2007 inclusive. This choice is based on a compromise between desirability of a long-as-possible comparison period, availability of ocean models, and temporal coverage by multiple satellite altimeter missions. Appendix 1 contains a sensitivity analysis of the epochs used to compute MSL at Australian tide gauges, showing the 2003-2007 epoch to be representative of the longer term mean.

2.1 MDT estimation approaches

Determination of the MDT can be through the ‘geodetic’ or ‘ocean’ approaches (Woodworth et al. 2012). The geodetic approach uses either:

- a) a MSS model obtained from satellite altimetry (e.g., Bingham et al. 2008, 2014; Andersen and Knudsen 2009; Knudsen et al. 2011; Schaeffer et al. 2012, Huang 2017), or
- b) mean sea level (MSL) observations at tide gauges expressed as ellipsoidal heights from co-located GNSS observations (e.g., Woodworth et al. 2015; Hughes et al. 2015; Lin et al. 2015).

In both of these geodetic approaches, a geoid model is subtracted from the MSS/MSL to derive the MDT. For (a), this may be done using a pointwise method (Jayne 2006; Bingham et al. 2008), where values of the geoid are subtracted from the MSS. Alternatively, a spectral method can be used (Bingham et al. 2008), where spherical harmonic coefficients of the geoid are subtracted from spherical harmonic coefficients of the MSS to the same degree, although filtering is required to reduce the effects of Gibbs fringing. Bingham et al. (2008) found that the spectral method provided better results than the pointwise method. For (b), MDT is realised only at discrete locations. Tide gauges provide direct observations of MSL, but the method is dependent on reliable ties to a nearby benchmark with GNSS observations, as well as the quality of the gravimetric geoid model at the tide gauge location. The lack of tide gauge and related infrastructure is often a limitation for LVD unification from tide gauges (e.g., Woodworth et al. 2015), which requires large numbers of evenly spaced tide gauges to provide redundancy.

The ocean approach uses either:

- c) *in situ* observations of surface currents, temperature and salinity to infer the MDT from hydrodynamics (e.g., Cartwright and Crease 1963; Amin 1988; Ridgway et al. 2002; Dunn and Ridgway 2002), or
- d) a global numerical ocean model using physics-based dynamical constraints to compute the MDT (e.g., Marshall et al. 1997a, 1997b; Menemenlis and Wunsch 1997; Menemenlis et al. 2005).

Global ocean models used in (d) are designed primarily for use in deep oceans, rather than at the coast and in shallow continental shelves. Woodworth et al. (2012) discuss the deficiencies of ocean models for coastal MDT, but postulated that an ocean model may provide realistic coastal MDT estimates if forcing factors are well modelled, and the model is of high spatial and temporal resolution. Some ocean models assimilate other data, including geodetic data, in order to constrain them to be closer to reality than the approximate model physics alone would allow. We distinguish between ocean models (class d) by the sub-classifications: (d1) models that do not assimilate geodetic information and are therefore considered independent ocean models (IOM), and (d2) those

that do assimilate geodetic information and thus are non-independent ocean models (NIOM). Note that we are referring to the independence of the ocean models to geodetically derived MDT, not independence among the ocean modelling component of the IOM and NIOM.

A final classification (e) of MDT models refers to a combined method incorporating ocean information to supplement the altimetry MSS and geoid (geodetic) information. These combined MDTs usually take the difference between an altimetry-derived MSS and a geoid model as a first approximation, then adjust it by including observed oceanographic information. Details of the methods are in, e.g., Rio and Hernandez (2004), Maximenko et al. (2009) and Rio et al. (2011, 2014).

2.2 Altimetry MSS minus gravimetric geoid model (a)

Only one geodetic MDT of class (a) is used here because our focus is on testing multiple ocean models (Section 2.4). It is determined from the TUM13 gravimetric geoid (Fecher et al. 2015) subtracted from the altimeter-derived DTU10MSS (Andersen and Knudsen 2009; Knudsen et al. 2011), and referred to herein as DTU10MSS minus TUM13. TUM13 is provided to spherical harmonic degree 720, and uses data from GOCE in the low to medium wavelength component, with a contribution from GRACE. The higher frequency components of the geoid are provided by terrestrial and altimeter-derived gravity anomalies.

The DTU10MSS is an average over the period 1993-2009, but is mapped to the 2003-2007 average by using the difference in AVISO (Archiving, Validation, and Interpretation of Satellite Oceanographic data) absolute dynamic topography (ADT) averages over the two periods. In this case, DTU10MSS was used rather than DTU13MSS because DTU10MSS is consistent with the TUM13 geoid (the gravity anomaly dataset is derived from DTU10MSS, so the difference does not add artificial small scale errors into the dynamic topography), and also, as stated in Woodworth et al. (2015), there are known problems with some coastal values in the DTU13MSS.

Note that, with the exception of the time-variable GRACE models, geoid models are not normally accompanied by a stated epoch. Instead, satellite-only gravity data are averaged over the missions' durations, altimeter-derived gravity data are stacked from multiple missions over the past ~20 years, and land gravity data depend on the date of the surveys. The latter have been available since the 1950s when the portable gravimeter was developed.

Special care was taken with the spectral matching (cf. Bingham et al., 2008) of the DTU10MSS and the TUM13 geoid. The latter was based on a combination of satellite data and (over the ocean) $\frac{1}{4}$ degree block averages of gravity anomalies determined from the DTU10MSS, with the $\frac{1}{4}$ degree scale chosen to match the expansion to degree 720 used in the geoid product. Here, we use matched $\frac{1}{4}$ degree block averages of the geoid expanded to degree 720 and of the DTU10MSS. This produces, before any filtering, a much cleaner MDT than is typically found when combining truncated geoid data and a MSS (cf. Bingham et al. 2008). We then identify typical MDT noise characteristics by assuming noise to be the cause of all the variability, using a region of the tropical Pacific that is known to have a smooth MDT. This is used, together with a signal variance estimated from the NEMO12a model MDT (Table 1), to derive a Wiener filter that further reduces noise. Tests using model-independent sea surface temperature data to construct the expected signal variance produced very similar results, typically within 10 mm.

The process used to extrapolate DTU10MSS minus TUM13 MDT to the tide gauge locations (Fig. 1) is similar to that described in Hughes et al. (2015), but better adapted to the individual model grids. Any model values that were more than one grid-cell distant from the coast were removed. The remaining model coastal values were mapped to the nearest point identified as coastal on the 0.5 arc-minute gridded GEBCO (General Bathymetric Chart of the Ocean; <http://www.gebco.net/>) bathymetry). These coastal points were then checked to ensure that they were in the same order as the model points around the coast. Where that was not the case, or where multiple model coastal points were mapped to the same fine-resolution coastal point, they were re-ordered and spread to

equal alongshore distances between the surrounding, correctly mapped points. MDT at the tide gauge location was then calculated by linearly interpolating along the line of GEBCO coastal grid points to the point closest to the tide gauge's latitude and longitude.

2.3 Tide gauge MSL geodetic MDT (b)

This estimate of coastal MDT is determined through a discrete observation of MSL at a tide gauge, with a geoid height subtracted from the MSL at the tide gauge location (e.g., Woodworth et al. 2012, 2015; Hughes et al. 2015; Filmer 2014). We use available geoid or quasigeoid models: Australian gravimetric quasigeoid 2009 (AGQG2009; Featherstone et al. 2011) and Earth Gravitational Model 2008 (EGM2008; Pavlis et al. 2012, 2013). In addition, we use the TUM13+EGM2008 geoid, which is distinct from TUM13 used in the altimetric MSS ((a) in Section 2.2). In this case, the TUM13 geoid is extended beyond degree 720 by using spherical harmonic coefficients from EGM2008, and the resulting extended geoid calculated to its full resolution (degree 2190) in order to obtain the point values necessary for tide gauge MDT determination. In this case, there is no filtering.

The ellipsoidal height of MSL is determined from GNSS observations at benchmarks near the tide gauge (described below). Sea level data and tide gauge locations (given to the nearest arc-minute of latitude and longitude) are from the Permanent Service for Mean Sea Level (PSMSL; Holgate et al. 2013). MSL was corrected for atmospheric pressure to obtain sea level on an isobaric surface using a standard air pressure of 1011.4 mbar (e.g., Wunsch and Stammer 1997) utilising data from the National Centers for Environmental Prediction-National Center for Atmospheric Research reanalyses (Kistler et al. 2001). The nodal tide has not been removed, but the effect is less than ~10 mm (Woodworth 2012), so is not considered here. Only MSL data classified by the PSMSL as revised local reference (RLR) information was used. RLR MSL data have been referenced to local benchmarks, so have consistent vertical datum stability through time (Holgate et al. 2013).

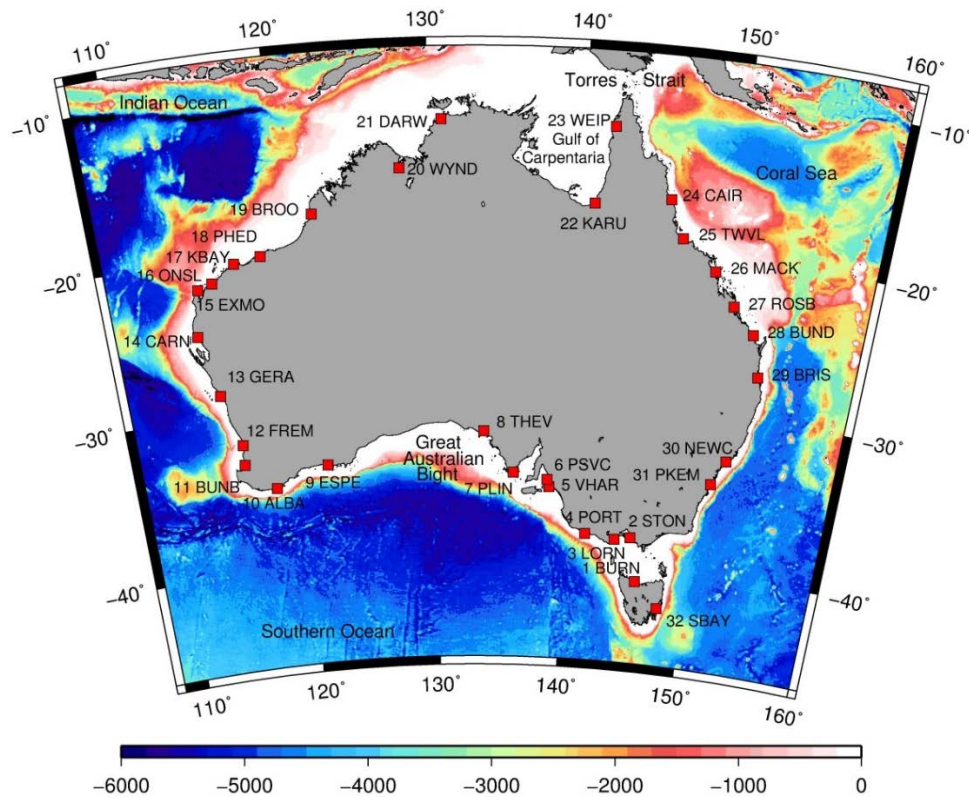


Fig. 1: The 32 Australian tide gauges used in this study, shown as red squares. Numbers are designated and used in later Figs. See Table A2 of Appendix 2 for details of each gauge. Bathymetric data is in metres and obtained from http://topex.ucsd.edu/cgi-bin/get_data.cgi (Smith and Sandwell 1997).

Ellipsoidal heights come from GNSS observations at benchmarks at or near the tide gauges (Fig. 1 and Appendix 2). Episodic GNSS observations for 29 of the tide gauges were provided by Geoscience Australia (N. J. Brown, pers. comm. 2009). These data were processed by Hu (2009) in the International Terrestrial Reference Frame 2005 (ITRF2005; Altamimi et al. 2007) at epoch 2000.0. More recent episodic GNSS observations for three tide gauges were provided by the Western Australian State Government geodetic agency Landgate (L. M. Morgan, pers. comm. 2015) and processed in Geoscience Australia's AUSPOS online processing software (<http://www.ga.gov.au/bin/gps.pl>) in ITRF2008 at epochs during 2012–2013. The 29 ITRF2005 coordinates were transformed to ITRF2008 using transformation parameters from http://itrf.ensg.ign.fr/ITRF_solutions/2008/tp_08-05.php (Altamimi et al. 2011). The transformation amounted to no more than 3 mm in ellipsoidal height. All 32 ITRF2008 ellipsoidal heights were then aligned to epoch 2005.5 as the midpoint of the 2003–2007 (2003.0–2008.0) period used for the MSL (Appendix 1). This was done using site velocities from the nearest APREF GNSS station (Asia-Pacific Reference Frame; <http://www.ga.gov.au/scientific-topics/positioning-navigation/geodesy/asia-pacific-reference-frame>) as a proxy for an assumed linear velocity of each ellipsoidal height. The maximum change in the ellipsoidal heights from the observation/processing epoch and reference frame transformation was 10 mm, but most were <5 mm.

AVISO and DTU10MSS minus TUM13 MDTs (Table 1) are in the mean tide system. AGQG2009 and EGM2008 are in the tide-free system (N_{TF}), as are the GNSS ellipsoidal heights (h_{TF}) (G. R. Hu, pers. comm. 2012), so these were converted to mean tide (N_{MT} and h_{MT} respectively) so that all MDTs were in the same permanent tide system (cf. Ekman 1989). The geoid models were converted $N_{MT} = N_{TF} + A_0(1 + k_2)$, and the GNSS ellipsoidal heights $h_{MT} = h_{TF} + A_0h_2$, where $A_0 = D \left(\frac{1}{3} - \sin^2\phi \right)$, with ϕ the tide gauge latitude, $D = 29.767$ cm, $k_2 = 0.3019$, and $h_2 = 0.6078$ (Petit and Luzum 2010).

The ellipsoidal height of MSL (h_{MSL}) at the tide gauge is determined using the following method (cf. Woodworth et al. 2012; Filmer 2014). The levelled height difference (ΔH) between the GNSS site and the tide gauge is usually the only available connection. The ellipsoidal height between the GNSS and tide gauge (Δh) is derived as $\Delta h = \Delta H + \Delta N$, where ΔN is the difference between the geoid at the tide gauge and the GNSS site. Thus, $h_{MSL} = (h_{GNSS} - (\Delta H + \Delta N)) - H_{RLR} + MSL_{RLR}$, where h_{GNSS} is the measured ellipsoidal height at the GNSS site, H_{RLR} is the vertical distance from the tide gauge to RLR and MSL_{RLR} is the height of MSL above RLR for the specified epoch. We then use $MDT = h_{MSL} - N_{TG}$ (geoid height at the tide gauge) to obtain geodetic MDT at the tide gauge.

Distances from GNSS benchmarks to the tide gauges are shown in Appendix 2 (Table A2). The maximum distance is ~5 km, with 19 out of 32 <1 km from the tide gauge, and the average ~1.1 km. This levelling is likely to be ICSM (2007) Class LC levelling with maximum allowable tolerance $12\sqrt{d}$ mm where d is the distance of the levelling run between benchmarks in km. Filmer et al. (2014) found Class LC levelling in the Australian National Levelling Network (ANLN) to have a standard deviation of $\sim 5\sqrt{d}$ mm from variance component estimation, so if this is propagated over 5 km, we estimate that the maximum error from the levelling connection will be ~11 mm, but ~5 mm on average (see Section 2.6 for an error estimate of geodetic MDT at tide gauges).

2.4 Ocean approaches (c and d)

The CARS2009 (Commonwealth Scientific and Industrial Research Organisation (CSIRO) Atlas of Regional Seas; Dunn and Ridgway 2002; Ridgway et al. 2002) was developed from observations in the open ocean and is only available for open ocean regions deeper than 2000 m (Fig. 1). To determine the MDT value at the tide gauges, CARS2009 data were re-gridded using the Generic Mapping Tools (GMT; Wessel et al. 2013) surface routine of Smith and Wessel (1990), so that the CARS2009 MDT could be extrapolated to the coast. Bicubic interpolation from this extended grid

was used to give CARS2009 MDT at each tide gauge's latitude and longitude. The epoch of CARS cannot be clearly defined, as it was computed from ocean observations over the past 50 years, although weighted towards the larger amount of observations from the past two decades.

Each of the 13 numerical ocean models (class d; Table 1) have been averaged over the five-year period 2003-2007. The models have been grouped according to independence from assimilated geodetic information (IOM (d1), or NIOM (d2)). Although the models span a wide range of resolutions, formulations and data sources, there do remain some elements of commonality. None of the models include tides or waves, and there may be common errors in the meteorological forcing fields (though these come from a variety of different sources). The ocean model MDTs were computed at the tide gauge location using the method described for the DTU10MSS minus TUM13 MDT (Section 2.2). We include a large number of ocean models in the study so that each can be tested and evaluated in the variable conditions encountered at the different tide gauge locations around Australia. This avoids the risk of discarding some models prior to testing, that may otherwise perform well in these differing locations, and illustrates the range of behaviours found in different kinds of model.

MDT	Spatial resolution	Epoch	Remarks
a) Altimetry MSS minus gravimetric geoid model			
DTU10 MSS minus TUM13 geoid	1/12°	1993-2009 for MSS. Geoid epoch not specified (see Section 2.2).	DTU10 MSS (Andersen and Knudsen 2009, Knudsen et al. 2011) minus TUM13 (Fecher et al. 2015). Refer to Section 2.2.
b) Tide gauge MSL from http://www.psmsl.org/data/obtaining/ minus gravimetric geoid model			
MSL minus AGQG09 quasigeoid	1/60°	2003-2007 for MSL. Geoid epoch not specified (see Section 2.2).	Australian gravimetric quasigeoid 2009 (AGQG2009; Featherstone et al. 2011). The geoid and quasigeoid are identical at sea.
MSL minus EGM2008 geoid	1/12°		Earth gravitational model 2008 (EGM2008; Pavlis et al. 2012, 2013).
MSL minus TUM13+EGM2008 geoid	1/12°		TUM13 (Fecher et al. 2015) supplemented to degree 2190 using EGM2008, as per Hughes et al. (2015) and Woodworth et al. (2012, 2015).
c) Observations of currents, temperature and salinity			
CARS2009	1/4°	Uses data from ~ last 50 years.	Climatology from ocean observations (http://www.marine.csiro.au/~dunn/cars2009/) (Ridgway et al. 2002; Dunn and Ridgway 2002)
d) Global numerical ocean MDT model			
d1) Independent ocean models (IOM)			
NEMO12a	1/12°	2003-2007	Blaker et al. (2014). National Oceanography Centre, UK, model run. Tripolar ORCA grid. Initialised with climatological temperature and salinity. Run from 1978 to 2010 inclusive, forced by atmospheric reanalysis data for wind stress, temperature and freshwater fluxes. Model run has several restarts following minor code changes.
NEMO12b	1/12°		Blaker et al. (2014). New run of the same model as NEMO12a, but run without any code changes from 1958 to 2012 inclusive.
NEMO-Q	1/4°		Blaker et al. (2014). A model run similar to NEMO12b, but at lower spatial resolution and ending with the year 2007.
LIVS	1°		Woodworth et al. (2012). The Massachusetts Institute of Technology (MIT) model, run as an ocean analysis method, relaxing each year to the Hadley Centre ocean temperature and salinity field. Each year is started afresh. Resolution is enhanced at the latitudes and longitudes of the North Atlantic. No Arctic.
LIVC	1°		Williams et al. (2014). Like LIVS, but a regular 1° grid. The grid is identical to ECCO-G (below), and so has no Arctic and a closed Torres Strait.

SODA	1/4° (average)		Carton and Giese (2008). Global reanalysis (version 2.2.4) based on the POP2 ocean model and the Simple Ocean Data Assimilation (SODA) system covering the period 1871 to 2010. Surface forcing from the NOAA-CIRES 20th Century Reanalysis (version 2c). Assimilates sea surface temperature and subsurface temperature and salinity, but not MDT.
GFDL	1° (reducing to 1/3° meridional spacing near the equator)		Chang et al. (2013). The coupled climate model CM2.1 with the MOM4 ocean component and the GFDL ensemble coupled data assimilation (ECDA) system covering the period from 1960 until present. Assimilates atmospheric temperature and winds and ocean temperature and salinity observations, but not MDT.
d2) Not independent ocean models (NIOM)			
ECCO2	~18 km	2003-2007	Menemenlis et al. (2005). Jet Propulsion Laboratory “cubed sphere” grid as part of the Estimation of the Circulation and Climate of the Ocean (ECCO) consortium. Includes data assimilation.
ECCO-G	1°		Köhl et al. (2007). MIT model run using version 3 of the ECCO-GODAE model. Has no Arctic, and the Torres Strait is closed. Assimilates a wide variety of ocean observations, including MDT.
ECCO4r2	~80km (1° at equator decreasing towards the poles)		Forget et al. (2015). Global state estimation from the ECCO consortium based on the MITgcm using the Lat-Lon-Cap (LLC) grid and covering the period 1992 to 2011. Surface forcing from the ERA-interim reanalysis. Assimilates a wide range of oceanographic observations, including MDT.
GLORYS	1/4°		Ferry et al. (2012). Global reanalysis (version 2.3) based on NEMOv3.1 ocean and LIM2 sea ice models covering the period 1993 to 2014 with surface forcing from the ERA-interim reanalysis. Assimilated ocean observations include temperature, salinity and MDT.
HYCOM	1/12°		Cummings and Smedstad (2013). Global reanalysis (GLBu0.08/expt_19.1) based on the HYCOM ocean model and the Navy Coupled Ocean Data Assimilation (NCODA) system covering the period 1995 to 2012. Surface forcing from the NCEP Climate Forecast System Reanalysis (CFSR). Assimilated ocean observations include temperature, salinity and MDT.
NEMO-UoR	1/4°		Valdivieso et al. (2014). Global reanalysis based on NEMOv3.2 ocean and LIM2 sea ice models and the UKMO (Meteorological Office) FOAM data assimilation system covering the period 1985 to 2010. Surface forcing from the ERA-interim reanalysis. Assimilated ocean observations include temperature, salinity and MDT.
e) Combined geodetic-ocean MDT model			
AVISO	1/4°	1993-1999 for MSS. Geoid epoch not	2014 reprocessing of the CNES-CLS13 MDT http://www.aviso.altimetry.fr/en/data/products/auxiliary-products/mdt.html .

		specified (see Section 2.2).	
--	--	---------------------------------	--

Table 1: Summary of MDT models classified among geodetic, ocean and combined approaches.
The spatial resolution given in (b) refers to that of the corresponding geoid model.

2.5 Combined geodetic-ocean MDT model (e)

Combined geodetic-ocean MDT models take a first estimate of MDT by subtracting a geoid model from an altimetric MSS. This first estimate is then adjusted by the introduction of ocean observations (e.g., Rio and Hernandez 2004; Rio et al. 2011; Maximenko et al. 2009). The combined geodetic-ocean MDT model referred to herein as AVISO is a 2014 reprocessing of the CNES-CLS13 MDT of Rio et al. (2014). It combines the CNES_CS11 global MSS (Schaeffer et al. 2012) from altimetry, the EGM-DIR R4 geoid model (Bruinsma et al. 2013), and *in situ* ocean observations to determine the short-wavelength MDT (Rio et al. 2014). To obtain the 2003-2007 epoch, we use the AVISO ADT product that combines the MDT with temporal anomalies to give daily values of the total dynamic topography, which were averaged over the years 2003-2007 (as per Section 2.2). The method of computing AVISO MDT values at tide gauges is the same as for the ocean models and DTU10MSS minus TUM13 (Section 2.2).

2.6 MDT errors at Australian tide gauges

The uncertainty associated with the determination of the model MDTs at tide gauges must be considered. Firstly, the tide gauge location is only given to the nearest 1 arc minute (implying an uncertainty of ± 30 arc seconds, or ~ 0.8 km at 25°S , which is approximately the mean latitude for Australia). This means that the location of the geoid heights, ocean models and altimetric geodetic MDT can only be estimated within the tide gauge location uncertainty. Thus, any large changes in the MDT value within this region may propagate into the MDT comparison at the tide gauge location. Featherstone and Filmer (2012) tested the variation of the interpolated CARS2009 MDT within a ~ 1 km radius of the same tide gauges used here, finding the maximum error to be no more than a few cm.

The MDT models in Table 1 are of various spatial resolutions, ranging from 1 arc-degree (~ 100 km at 25°S) to 1/12 of an arc-degree (~ 8 km at 25°S), so that each grid value represents a larger spatial scale than sea level recorded at the tide gauge location. The result of this is that the MDT model value computed at the tide gauge may only be representative of the open ocean at some distance away from the tide gauge.

It is difficult to quantify this error as none of the MDT models are accompanied by formally propagated error estimates. However, the comparisons conducted in Section 3 do go some way to providing upper and lower bounds. Previous studies around Australia (Featherstone and Filmer 2012; Filmer 2014) and in other regions (Woodworth et al. 2012; Hughes et al. 2015; Lin et al. 2015; Ophaug et al. 2015; Higginson et al. 2015; Mazloff et al. 2014; Idžanović et al. 2017) found standard deviation (SD) of differences among MDT models ranging from $\sim \pm 30$ mm to $\sim \pm 80$ mm. The resolution-induced (omission) errors discussed above are subsumed within these SDs, but will vary depending on the spatial resolution of the different models (Table 1). Additional guidance can be taken from Vinogradov and Ponte (2011), who found an RMS difference in MSS of $\sim \pm 20$ -40 mm among 15 Australian tide gauges and adjacent altimetry estimates (~ 80 km from the tide gauge) in a global study on interannual MSL variability.

A further indication of MDT error comes from Filmer et al. (2014), where a combined least-squares adjustment of heterogeneous height information (levelling, ellipsoidal h and geoid N , MSL and MDT at tide gauges) for Australia was conducted. Using variance component estimation (VCE), the SD of the combined MSL and MDT constraint was ± 82 mm, with the VCE uncertainty ± 13 mm, based on the equations of Teunissen and Amiri-Simkooei (2008). The MSL values used were those observed at tide gauges during 1966-1968 (for the definition of the Australian Height Datum; AHD; Roelse et al. 1971), while CARS2009 provided the MDT component. Using average MSL variability over five years

(Appendix 1) as a guide, the MSL error contribution for the three-year average MSL may be $\sim\pm 20$ -40 mm, suggesting the CARS2009 component of this combined error to be $\sim\pm 50$ mm.

The CARS2009 climatology is more susceptible to coast-ocean decoupling than some other ocean MDTs because it consists of steric sea level information referenced to 2000 m depth in the open ocean (cf. Bingham and Hughes 2012). Thus, CARS2009 requires extrapolation from some way offshore across the broad continental shelf of northern Australia to the coast (see Fig. 5a in Featherstone and Filmer 2012), and does not account for shallow water and barotropic processes in regions such as the Gulf of Carpentaria (Fig. 1).

We conclude this section with an approximate error estimate for geodetic MDT at tide gauges. The levelling error for the average distance from the GNSS site to the tide gauge (1.1 km; from Section 2.3) is $\sim\pm 5$ mm. The average of the SD from the 32 processed GNSS heights is ± 16 mm (from Table A2; SD from the processing scaled by 10 (Rothacher 2002)), which we use as a proxy for the estimated uncertainty. The error from the geoid models is estimated as $\sim\pm 70$ mm (see Fig. 7 in Section 4 of this paper; Pavlis et al. 2012) at the tide gauges, and the relative geoid difference error from GNSS site to the tide gauge (maximum 5 km, but mostly <1 km) may be $\sim\pm 20$ mm. If we consider the MSL error to be $\sim\pm 20$ mm (including residual nodal tide), we can use linear error propagation assuming independence to cautiously estimate an uncertainty for the geodetic tide gauge MDT of $\sim\pm 92$ mm. The empirical estimates from other studies described in this sub-section suggest the ocean model MDT error to be $\sim\pm 50$ mm. This is qualified by variability among the different contributing error sources at different locations.

3 Results

A comparison is made at 32 Australian tide gauges (Fig. 1) among (a) DTU10 MSS minus TUM13 geoid, (b) three tide gauge MSL minus gravimetric geoid models, (c) CARS2009, (d) 13 numerical ocean model MDTs, comprising seven IOM (d1) and six NIOM (d2), and (e) the AVISO combined geodetic-ocean MDT (Table 1). Firstly, we present results comparing all MDTs, describing the general behaviour of the coastal MDT around Australia.

3.1 Australian coastal MDT

To evaluate relative differences among the coastal MDT profiles for visual comparison in Figs. 2-5, the mean value (for all 32 tide gauges) for all of the 13 ocean models was computed (as a proxy for a regional mean), to which all MDTs were referenced. This also highlights the MDT variability at different tide gauges with respect to a mean value, which would be needed for VDU of the Australian continent. As a guide to possible outliers, the mean and SD of all MDTs for each tide gauge were computed. To avoid biased SDs at tide gauges with large differences among MDTs (e.g., tide gauges #18 and #20 in Fig. 2), the mean of the SDs for all tide gauges was computed (± 46 mm) as a proxy for the unknown error. Assuming a normal distribution, this mean SD was then scaled to the 99% confidence level (factor of 2.58) for all tide gauges (± 118 mm). This is used as a proxy to identify “outliers” or anomalies relative to the mean value for MDT at each tide gauge. Figures 2-5 show the 99% confidence bounds as black dotted lines so that MDT values on, or outside, these bounds can be interrogated further. Note that MDT differences between tide gauge pairs are used for statistical analysis in Tables 2a, 2b and 3.

There is broad agreement among all MDTs (Fig. 2), but with differences reaching ~ 200 mm at some tide gauges. There is a general increase in MDT from tide gauge #1 (BURN; Fig. 1) on the island of Tasmania, increasing ~ 100 mm along the south coast of Australia to tide gauge #8 (THEV), and a further ~ 100 mm to tide gauge #10 (ALBA), near the south west corner of Australia. This increase between THEV and ALBA may be due to the Leeuwin Current moving closer to shore around the south western coast, so that the signal

is observed at the tide gauges, before moving further offshore as it crosses the Great Australian Bight (cf. Ridgway and Condie 2004; Ridgway and Godfrey 2015).

MDT increases steeply along the west coast from #10 (ALBA) to #15 (EXMO), before increasing more slowly to #21 (DARW). The steep, large-scale slope, of about 2×10^{-7} , is significantly larger than that observed along other oceanic eastern boundaries, where (excepting the Strait of Gibraltar, which is not a true boundary) slopes are at most about 1×10^{-7} (Woodworth et al. 2012). Between EXMO and DARW, significant features are two ‘spikes’ of up to ~200 mm for the tide gauge geodetic MDT (using AGQG2009, EGM2008, and TUM13+EGM2008 geoids) that appear at #18 (PHED) and #20 (WYND). Neither indicates any correlation with the ocean models, although the DTU10MSS minus TUM13 MDT does replicate this feature at WYND. All are on or outside the 99% confidence bound in Fig. 2. This is discussed further in Sections 3.3 and 4. Tide gauges #22 (KARU) and #23 (WEIP) are situated in the Gulf of Carpentaria, and show a drop of ~100 mm from DARW.

MDT climbs (~200 mm inferred by most ocean models) from #23 (WEIP) to #24 (CAIR), which is on the eastern side of the Torres Strait (Fig. 1). Wolanski et al. (2013) suggest that net east-west flow through the Torres Strait (connecting the Gulf of Carpentaria and the Coral Sea) is negligible, but that a wind-driven increase in MSL on the Coral Sea side is countered by an opposing wind-driven effect causing lower sea level on the Gulf of Carpentaria side of the Torres Strait. This provides some explanation for the apparently large gradient between WEIP and CAIR shown in Fig. 2. The very shallow Torres Strait (<20 m; Wolanski et al. 2013) provide a significant barrier to the flow of water, allowing a difference in MDT to be maintained.

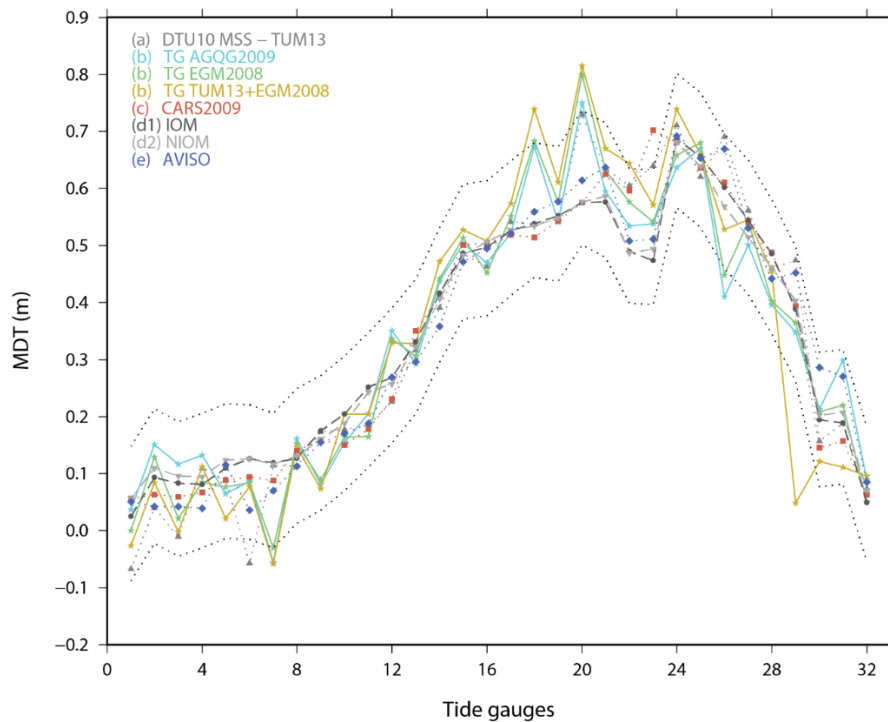


Fig. 2: MDT profiles at 32 tide gauges (numbered as per Fig. 1) for the period 2003-2007. MDT classifications are as per Table 1; (a) altimetric MSS geodetic MDT are triangles with dotted lines; (b) tide gauge geodetic MDT are stars with solid lines; (c) ocean observations are squares with dotted lines; (d) ocean models are dashed lines, with IOM (d1) as circles and NIOM (d2) as inverted triangles (average of all IOM and NIOM shown separately); (e) combined geodetic-ocean MDT are diamonds with dotted lines. Colours for each MDT are as per the legend. Tide gauges are clockwise from tide gauge #1 (BURN; see Fig. 1). All MDT profiles have been adjusted to have the same mean, so differences are relative. Black dotted lines are 99% confidence from the mean MDT value at each tide gauge.

MDT decreases along the east coast of Australia (cf. Hamon and Greig 1972; Mitchell 1975) to #30 (NEWC), after which a jump appears from #30 to #31 (PKEM). The East Australian Current (EAC) runs along the east coast of Australia, but the jump (varying magnitude) for all MDTs at PKEM suggests that the EAC reaches the coast at this point (cf. Ridgway and Dunn 2003). Ridgway (2007) suggests that there have been long-term variations in the EAC, in addition to seasonal variations, which may contribute to the variable results among the MDTs. South of PKEM, MDT decreases sharply to #32 (SBAY) on the east coast of Tasmania. These steep slopes along the oceanic western boundary are consistent with those seen along the Atlantic western boundary (Woodworth et al. 2012).

To compare MDTs statistically, we use the ocean model MDT (d) inferred sea slope differences ΔMDT_{TG}^{OM} between all combinations of tide gauge pairs (496 differences for 32 tide gauges). These are then subtracted from the difference of the corresponding tide gauge pair for (1) the mean of all other non-numerical ocean model MDT (classes a, b, c, e) ΔMDT_{TG}^{MNOM} , which is assumed representative of a group of semi-independent MDTs; (2) CARS2009 (c) ΔMDT_{TG}^{CARS} shown by Featherstone and Filmer (2012) to be the most effective MDT to account for the tilt in the AHD; and (3) AVISO (e) ΔMDT_{TG}^A which is based on a recent combined ocean-geodetic MDT. The statistics in Tables 2a and 2b are thus computed as (1) $\Delta MDT_{TG}^{MNOM} - \Delta MDT_{TG}^{OM}$, (2) $\Delta MDT_{TG}^{CARS} - \Delta MDT_{TG}^{OM}$, and (3) $\Delta MDT_{TG}^A - \Delta MDT_{TG}^{OM}$ among all combinations of tide gauge pairs. The sea slope differences between tide gauges are used in this instance because they provide more robust statistics than using an arbitrary mean (used for plotting in Figs. 2-5). However, using all MDT differences between tide gauges may tend to overestimate the SD if there are large errors in one or more of the MDTs compared.

MDT minus IOM (d1)		NEMO 12a	NEMO 12b	NEMO- Q	LIVS	LIVC	GFDL	SODA
(1) Mean of all non-ocean model MDT (a), (b), (c), (e)	SD	±0.052	±0.056	±0.060	±0.111	±0.085	±0.063	±0.044
	Max	0.184	0.186	0.204	0.378	0.228	0.140	0.123
	Min.	-0.089	-0.107	-0.129	-0.340	-0.276	-0.194	-0.102
(2) CARS2009 (c)	SD	±0.062	±0.072	±0.077	±0.125	±0.101	±0.069	±0.066
	Max	0.273	0.300	0.333	0.477	0.356	0.224	0.236
	Min	-173	-0.193	-0.266	-0.455	-0.381	-0.277	-0.236
(3) AVISO (e)	SD	±0.070	±0.073	±0.062	±0.088	±0.065	±0.063	±0.047
	Max	0.258	0.242	0.200	0.322	0.185	0.237	0.156
	Min	-0.117	-0.123	-0.121	-0.231	-0.160	-0.172	-0.115

Table 2a: Descriptive statistics (metres) for each of (1) the mean of all non-ocean model MDTs (a, b, c, e); (2) CARS2009 and (3) AVISO minus each independent ocean models (IOM). All statistics are computed from MDT-inferred sea slope differences between tide gauge pairs as defined in the text.

Table 2a contains comparisons for the IOMs (d1) and 2b the NIOMs (d2), demonstrating which ocean model shows best agreement with the MDT used here as ‘control data’ in (1), (2) and (3). For comparisons with (1), all values for tide gauges PHED, WYND and PLIN are removed to avoid the spikes in the geodetic MDT (a) and (b) introducing a bias into these SDs, while all 32 tide gauges are used in the comparisons with CARS2009 and AVISO, as these do not have obvious spikes in Fig. 2.

The statistical comparison (Table 2a, 2b) to the mean of all non-numerical ocean model MDTs (a, b c, e) indicates the closest agreement with SODA (SD ± 44 mm), NEMO12a (SD ± 52 mm), ECCO2 (SD ± 53 mm), and Nemo-UoR (SD ± 53 mm). SODA also had the smallest range (224 mm). When compared to CARS2009, NEMO12a has the lowest SD (± 62 mm), followed by ECCO2 (SD ± 62 mm), and SODA (SD ± 66 mm). LIVS, LIRC (IOM) and ECCO-G (NIOM) show largest SD and ranges for both comparisons and are indicated as ‘outliers’ in Figs. 3 and 4. The overall larger differences with CARS2009 appear to be exacerbated by large slope differences across the Gulf of Carpentaria (discussed in Section 3.2).

SODA has the lowest SD (± 47 mm) and range in the comparison with AVISO, while ECCO-G has the largest SD and maximum differences, which seems to be consistent across all comparisons. The SD of differences between the mean of seven IOM and six NIOM (Fig. 2) at all 32 tide gauges was ± 22 mm (maximum difference 56 mm, minimum -65 mm), indicating general agreement between these two classes. The mean IOM (d1) and mean NIOM (d2) had a SD of differences from the mean of all non-numerical ocean model MDT (a, b, c, e) of ± 57 mm (maximum 183 mm, minimum -154 mm) and ± 53 mm (maximum 163 mm, minimum -145 mm), respectively.

MDT minus NIOM (d2)		ECCO2	ECCO-G	ECCO4r2	GLORYS	HYCOM	NEMO-UoR
(1) Mean of all non-ocean model MDT (a), (b), (c), (e)	SD	± 0.053	± 0.141	± 0.095	± 0.071	± 0.073	± 0.053
	Max	0.177	0.428	0.198	0.217	0.209	0.177
	Min.	-0.126	-0.461	-0.281	-0.159	-0.212	-0.109
(2) CARS2009 (c)	SD	± 0.068	± 0.159	± 0.081	± 0.085	± 0.083	± 0.071
	Max	0.292	0.548	0.194	0.328	0.304	0.305
	Min	-0.219	-0.549	-0.250	-0.296	-0.278	-0.230
(3) AVISO (e)	SD	± 0.063	± 0.108	± 0.114	± 0.063	± 0.059	± 0.064
	Max	0.234	0.365	0.342	0.209	0.234	0.220
	Min	-0.151	-0.318	-0.333	-0.113	-0.135	-0.113

Table 2b: Descriptive statistics (metres) for each of (1) the mean of all non-ocean model MDTs (a, b, c, e); (2) CARS2009 and (3) AVISO minus each non-independent ocean models (NIOM). All statistics are computed from MDT-inferred sea slope differences between tide gauge pairs as defined in the text.

3.2 Comparison among ocean models (d), CARS2009 (c) and AVISO (e)

All IOM (d1) and NIOM (d2) are plotted separately in Figs. 3 and 4. CARS2009 (c) and the combined geodetic-ocean MDT AVISO (e) are included for comparison. LIVS shows a jump at #6 (PSVC), which is situated in a narrow gulf region (Fig. 1; see Fig. 8 later), and which may be explained by the coarser spatial resolution of LIVS (Table 1).

There is relatively large divergence among all ocean models for the north Australian tide gauges, most noticeably at #22 (KARU) and #23 (WEIP) in the Gulf of Carpentaria. This region hosts large spatial and temporal variations in sea level, which are largely weather-driven. For example, Forbes and Church (1983) found a 0.75 m annual range of MSL at the Karumba tide gauge (south east corner of the Gulf of Carpentaria; Fig. 1; #22 KARU). An annual periodic sea level amplitude of ~0.4 m in the Gulf of Carpentaria was reported by Tregoning et al. (2008) from tide gauge observations and GRACE mass variations. Monsoon winds are the primary cause of this large annual sea level range.

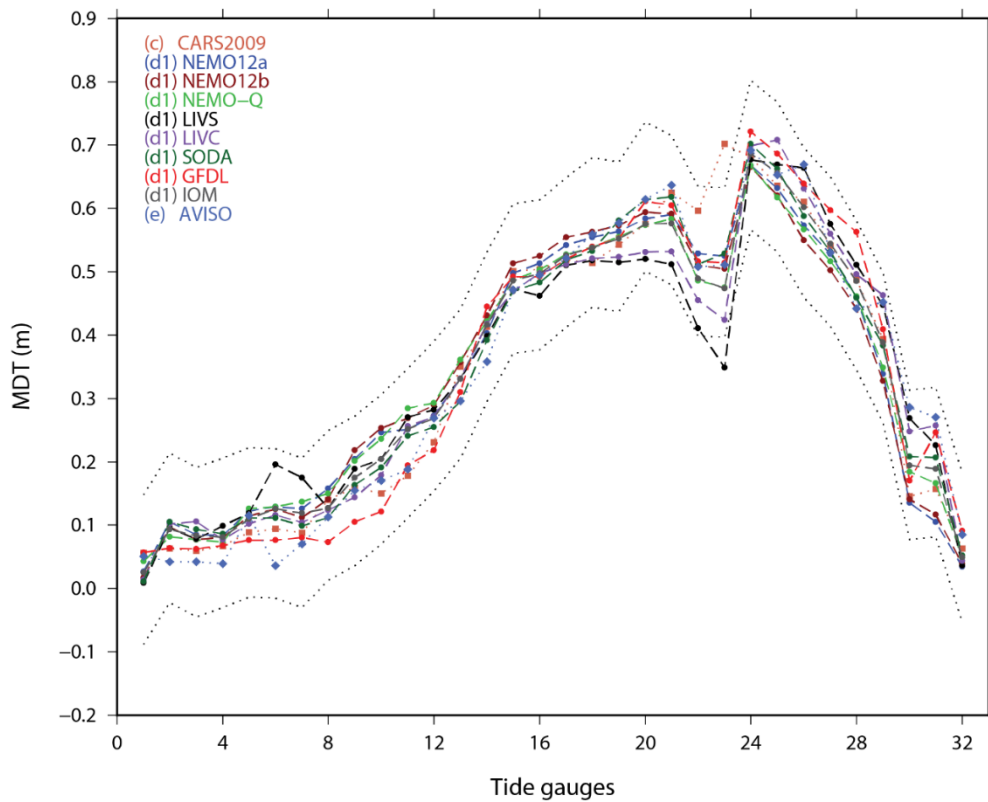


Fig. 3: MDT profiles at 32 tide gauges for the period 2003-2007 comparing: (d1) IOMs (dashed lines, circles) with IOM (average of all d1), (c) CARS2009 (squares with dotted lines), and (e) AVISO (diamonds with dotted lines). Colours are as per the legend. Tide gauges are clockwise and numbered from tide gauge #1(BURN; see Fig. 1). All MDTs have been adjusted to a common mean, so differences are relative. Black dotted lines are at 99% confidence from the mean MDT value at each tide gauge.

CARS2009 shows as an anomaly in the Gulf of Carpentaria (Figs. 3 and 4), outside 99% confidence at #23 (WEIP), which appears to be reflected in the statistics in Tables 2a and 2b. This is because the shallow seas in the Gulf of Carpentaria do not permit a reference depth of 2000 m and there is consequently no CARS2009 data in this region (cf. Fig. 5a in Featherstone and Filmer 2012). The agreement among tide gauge MSL minus AGQG2009, AVISO and several ocean models in the Gulf of Carpentaria suggest that CARS2009 does not represent MDT well in this region. Most ocean models agree with AVISO in this region (KARU and WEIP), although LIRC (d1), ECCO-G and ECCO4r2 (d2) differ from AVISO

but are outside the 99% confidence bound. ECCO4r2 is also close to the 99% confidence bound between tide gauge #9 (ESPE) and tide gauge #13 (GERA). Both LIVC and ECCO-G have a closed barrier across the Torres Strait (Table 1), which may account for the exaggerated gradient, especially in ECCO-G.

From Fig. 3, SODA appears to give a typical result. The low SDs for SODA seen in Tables 2a and 2b are therefore not the result of capturing particular features that are missed by other models. Overall, the comparisons suggest that higher model resolution helps, so the low SD of SODA may reflect a good balance between higher resolution than most assimilating models, and a less demanding assimilation method. By comparison, ECCO2 often also produces low SDs and has similar resolution to SODA, but uses an assimilation method that reduces the detailed impact of high-resolution data.

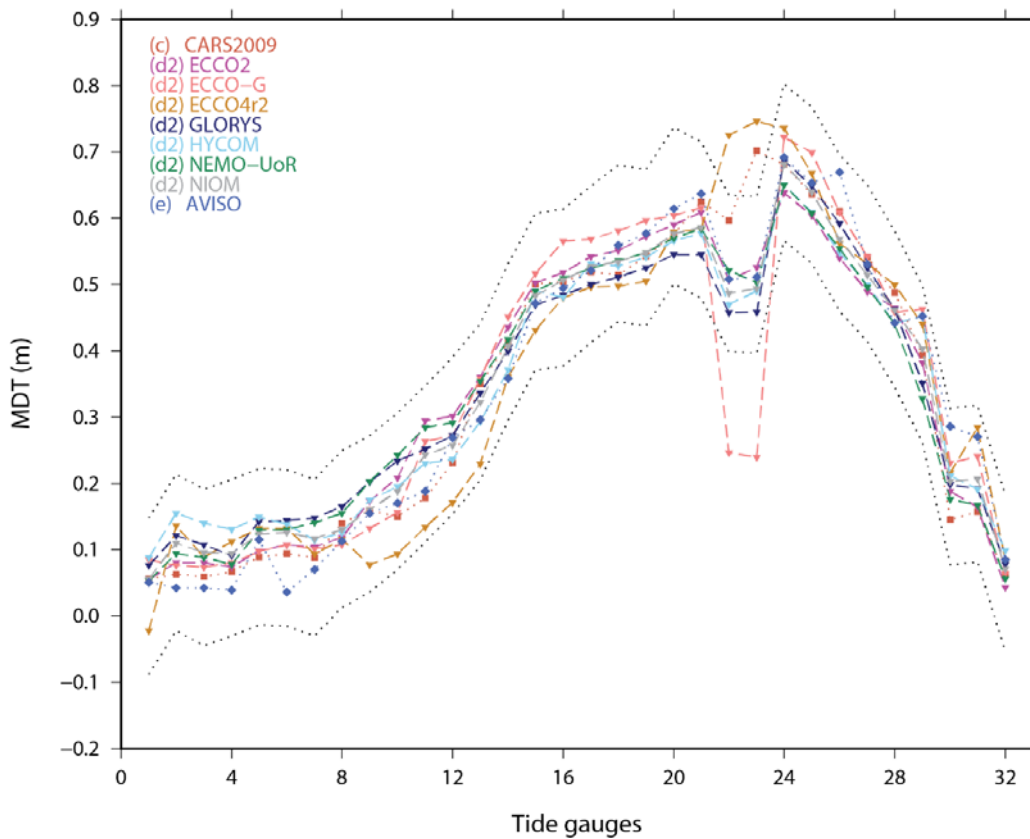


Fig. 4: MDT profiles at 32 tide gauges for the period 2003-2007 comparing: (d2) NIOMs (dashed lines, inverted triangle) with NIOM (average of all d2), (c) CARS2009 (squares with dotted lines), and (e) AVISO (diamonds with dotted lines). Colours are as per the legend. Tide gauges are clockwise and numbered from tide gauge #1(BURN; see Fig. 1). All MDTs have been adjusted to a common mean, so differences are relative. Black dotted lines are at 99% confidence from the mean MDT value at each tide gauge.

3.3 Altimetry (a) and tide gauge (b) geodetic MDTs

We compare altimetric geodetic MDT (a) and tide gauge geodetic MDT (b) with ocean models SODA, (d1) and ECCO2 (d2). These two ocean models are chosen for reference because they show the smallest SDs in the inter-model comparisons ($\sim \pm 50$ mm) in Section 3.2 (Tables 2a and 2b). The statistical analysis shown in Table 3 is computed using MDT-inferred sea slope differences between tide gauge pairs (as per Table 2a and 2b) from 29 tide gauges, providing 406 pairs. Tide gauges at PLIN, PHED and WYND are excluded from the comparison with geodetic MDT, as per Table 2a and 2b comparison (1).

The DTU10MSS minus TUM13 (a) in Fig. 5 (also see Table 3) shows broad agreement with the SODA and ECCO2 ocean models (d) for most of the Australian tide

gauges, but exhibits large differences at several locations. A ~ 150 mm drop at #6 (PSVC) may be due to the peninsular and island geography of this region (see Fig. 8 later), causing altimetry errors in DTU10MSS. This is only inferred because tide gauge MSL minus TUM13+EGM2008 agrees with other geodetic and ocean MDT at this tide gauge (see Section 4). This difference is due to an error in the coastal altimetry originating from the FES2014 tide model used in this region (O. B. Andersen, pers. comm. 2017). A ~ 150 mm spike is at #20 (WYND), but this tide gauge is located in an estuary some 40 km from the coast, which is in a gulf and so a further 30 km from the open ocean (see Fig. 9 later). DTU10MSS minus TUM13 does not follow the ~ 100 mm drop in the Gulf of Carpentaria suggested by the four ocean models and AVISO, but agrees more closely with CARS2009 through this region.

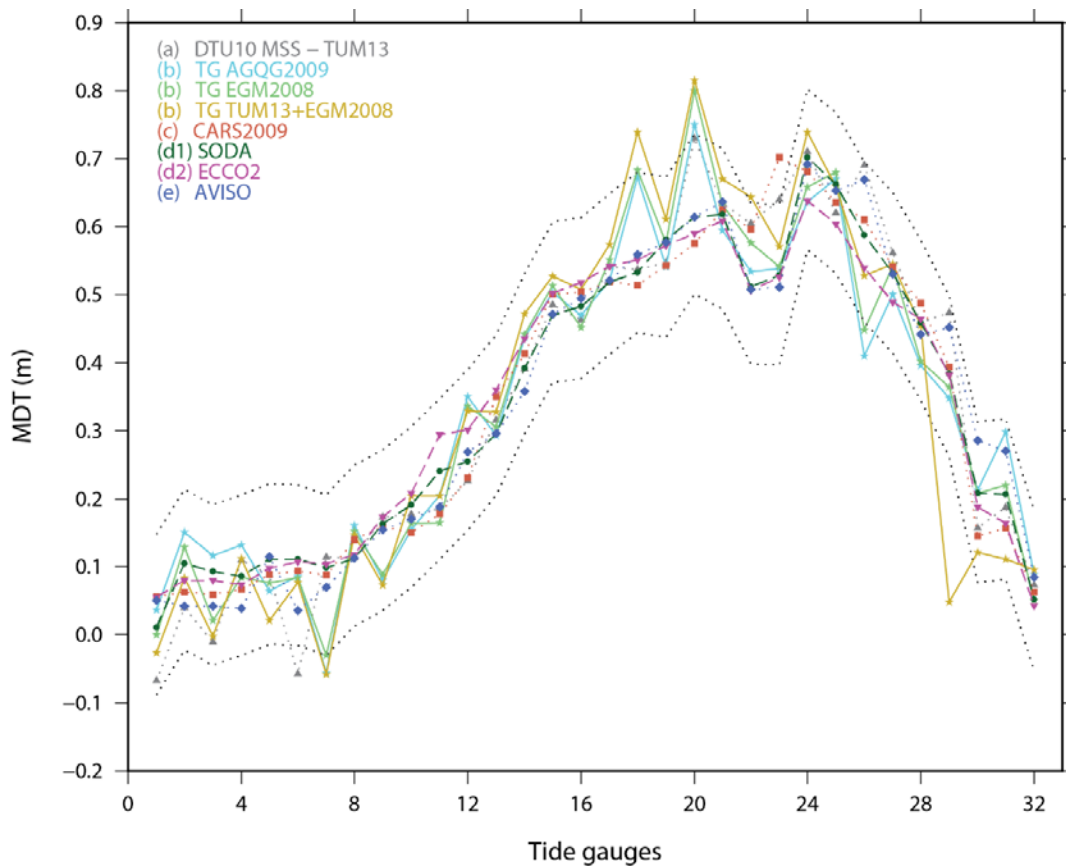


Fig. 5: MDT profiles at 32 tide gauges for the period 2003-2007 comparing (a) DTU10 MSS minus TUM13 (triangles with dotted lines), (b) tide gauge MSL minus: AGQG2009, EGM2008, and TUM13+EGM2008 (stars with solid lines). Also compared are (c) CARS2009 (squares with dotted lines), (d) ocean models (dashed lines) SODA, (d1; circles) and ECCO2 (d2; inverted triangles) and (e) AVISO (diamonds with dotted lines). Colours are as per the legend. Tide gauges are clockwise and numbered from tide gauge #1(BURN; see Fig. 1). All MDTs have been adjusted to a common mean, so differences are relative. Note that class (a), (b), (c), (e) in this Fig. are a subset of curves shown in Fig. 2. Black dotted lines are at 99% confidence from the mean MDT value at each tide gauge.

Tide gauge MSL minus AGQG2009 and tide gauge MSL minus EGM2008 geodetic MDTs (b) generally agree (Fig. 5 and Table 3), with the two largest differences at LORN (#3; 96 mm) and PKEM (#31; 78 mm), but neither of these are outside the 99% confidence bound. This agreement between AGQG2009 and EGM2008 (± 47 mm SD of differences between 406 tide gauge pairs) is expected as both models use the same altimeter-derived gravity data

and similar land gravity data (Featherstone et al. 2011; Pavlis et al. 2012, 2013). There are spikes at tide gauges #7 (PLIN), #18 (PHED), #20 (WYND) and #26 (MACK) compared to the ocean approach, and, in some cases, the altimetric geodetic MDTs. These will be investigated further in Section 4.

TUM13+EGM2008 shows the largest overall differences of the tide gauge MDTs, based on the statistics in Table 3. The SD of differences with SODA and ECCO2 are $\sim \pm 122$ mm with maximum and minimum differences $\sim +380$ mm and ~ -470 mm, respectively. A large drop also appears at #29 (BRIS) for the TUM13+EGM2008 MDT, which appears to be an error in the TUM13+EGM2008 geoid, as this is not seen in the EGM2008 and AGQG2009 tide gauge geodetic MDTs. This is confirmed by a direct comparison among these three geoid models at BRIS, where EGM2008 is $+0.016$ m compared to AGQG2009, but TUM13+EGM2008 is -0.301 m compared to AGQG2009. This is an example of using the ocean-model MDT as a diagnostic to identify possible coastal geoid errors.

MDT minus ocean model		SODA	ECCO2
DTU10 MSS minus TUM13 (a)	SD	± 0.078	± 0.088
	Max	0.279	0.314
	Min.	-0.192	-0.200
MSL minus AGQG2009 (b)	SD	± 0.078	± 0.081
	Max	0.269	0.264
	Min	-0.273	-0.201
MSL minus EGM2008 (b)	SD	± 0.067	± 0.071
	Max	0.157	0.204
	Min	-0.221	-0.178
MSL minus TUM13+EGM2008 (b)	SD	± 0.122	± 0.122
	Max	0.380	0.387
	Min	-0.468	-0.472

Table 3: Descriptive statistics of the differences among (a) altimetric geodetic MDT and (b) tide gauge geodetic MDT minus two ocean models: (d1) SODA and (d2) ECCO2 for 29 tide gauges. All statistics are computed from MDT-inferred sea slope differences between tide gauge pairs as defined in the text.

4 Discussion of Australian MDT profiles

Acknowledging a bias towards the more numerous ocean models in the mean of all MDTs at each tide gauge, we examine ‘outliers’ (or anomalies) that are outside of the 99% confidence bound (Section 3.1). This is important in the context of direct VDU using tide gauges, because using a large number of tide gauge constraints will contribute to a more robust

solution (e.g., Filmer et al 2014; Amjadiparvar et al. 2016), so that omitting tide gauges with large MDT errors reduces the number of tide gauges available for VDU. Conversely, the inclusion of MDTs containing large errors may bias the results in some regions. The following investigation into large MDT errors also contributes to the assessment and validation of the different MDTs tested.

Figure 5 suggests some outliers in the AGQG2009, EGM2008 and TUM13+EGM2008 tide gauge geodetic MDTs. Specifically, tide gauges #7 (PLIN), #18 (PHED), #20(WYND) and #26 (MACK) all show large (~150-200 mm) and consistent MDT differences from the ocean models, and are on or outside the 99% confidence bound. The difference at #29 (BRIS) has already been isolated to TUM13+EGM2008 (Section 3.3). Tide gauge #6 (PSVC) shows that DTU10MSS minus TUM13+EGM2008 is also outside the 99% confidence bounds.

Several possible causes for the differences at these tide gauges can be categorised as:

- 1) There are errors in all the ocean models, AVISO, and CARS2009, so that the tide gauge MSL minus geoid models are a correct representation of MDT;
- 2) The ocean models, AVISO and CARS2009 correctly represent MDT, but the geoid models (and DTU10MSS at PSVC) contain errors at the coast;
- 3) None of the ocean models, AVISO, CARS2009 and the geoid and MSS models contain large errors, but there is an error in the connection between the GNSS site and the tide gauge, or an undetected datum offset at the tide gauge. An error in the tide gauge connection, or relative geoid height (Sections 2.3 and 2.6) would affect all tide gauge geodetic MDT at that location, but the most notable outliers of this type (PLIN, PHED and WYND) are all <700 m from the tide gauge to the GNSS site.

It is also plausible that there is a decoupling between the sea surface offshore where sensed by altimetry, or modelled by the ocean approach, and the MSL observations at the tide gauges. However, Vinogradav and Ponte (2011) indicate that these differences were <40 mm for these regions, so we discount this as a cause of the outliers (>118 mm). In particular, we investigate the likelihood of possible causes (1) and (2) in the following.

Considering (1), the ocean models, AVISO and CARS2009 are sufficiently independent that it is unlikely that they would all be in good agreement at these four tide gauges, yet all be in error by the same magnitude. With the exception of WYND, and perhaps PLIN (see later), these tide gauge locations do not show complex coastal geography that may induce large magnitude MDT variations between the coastal and open ocean as indicated by the ocean models, AVISO and CARS2009. Hence, (1) seems to be a less likely cause of the larger differences at these tide gauges, and is therefore discounted.

The possibility of cause (2), concerning geoid errors at the coast, requires a more complex discussion. All gravimetric geoid models used to compute the geodetic MDTs have used largely the same altimeter-derived marine gravity anomalies in the coastal zone. Land gravity anomaly errors can also contaminate the geodetic MDTs, but this is less plausible than errors coming from the coastal altimeter data. AGQG2009 and EGM2008 both use DNSC08GRAV (Andersen et al. 2010) at 5- and 1-arc-minute resolutions, respectively, and TUM13 uses DTU10GRAV at 15-arc-minute resolution. Satellite altimetry is known to be poor in the coastal zone (e.g., Vignudelli et al. 2011), so affects the geodetic MDTs in two ways: (i) altimeter minus geoid MDTs will be affected by errors in both the altimetry MSS and the altimeter-derived gravity anomalies used in the gravimetric geoid model, and (ii) tide gauge MSL minus geoid MDTs will be affected by the geoid model computed from altimeter-derived gravity anomalies. In (i) however, correlated errors may cancel so any biases may not be so apparent. This is an example of the inseparability problem, but a

combination of ocean models and combined MDTs may infer whether tide gauge MDT are contaminated by geoid and/or MSS errors.

The DTU10MSS error grid (Fig. 6) demonstrates larger errors from altimetry MSS in the Australian coastal zone (cf. Deng et al. 2002; Claessens, 2012; Idris et al. 2014), when compared to the open ocean. These are not formally propagated errors, instead coming from the least squares prediction used to generate the MSS grid. EGM2008 is accompanied by a 5x5 arc-minute geoid error grid (http://earth-info.nga.mil/GandG/wgs84/gravitymod/egm2008/egm08_error.html) computed using the methods of Pavlis and Saleh (2005).

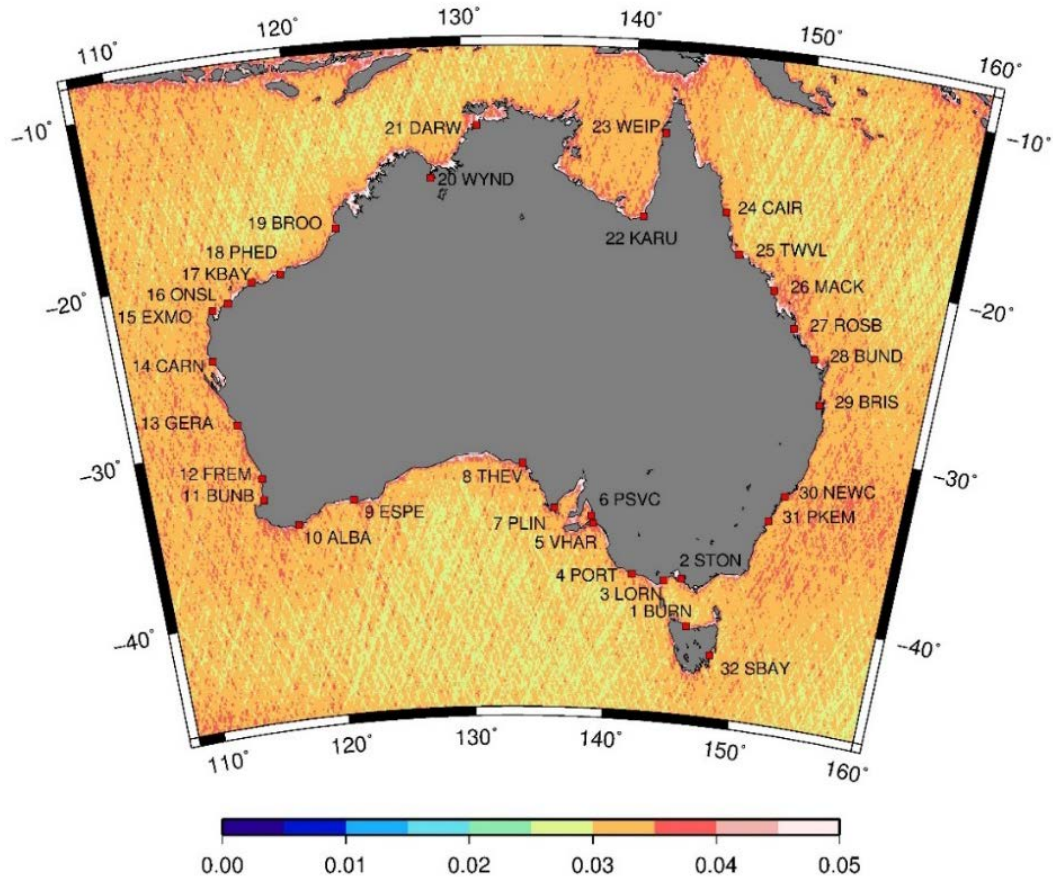


Fig. 6: The DTU10MSS error grid (metres) showing the interpolation error of the computed MSS from least squares prediction. Plotted from data downloaded from http://www.space.dtu.dk/english/Research/Scientific_data_and_models/downloaddata

Figure 7 shows error estimates for DTU10MSS and EGM2008 at the tide gauge locations, neither of which indicate errors of >70 mm in magnitude nor provide an explanation for the spikes in Fig 5. This suggests that either the EGM2008 and DTU10 MSS error grids are optimistic in some coastal regions, or that the geoid and/or altimetric MSS are not the primary cause of the differences to the ocean-model MDTs. No error grids are available for DNSC2008GRAV or DTU10GRAV, so we use the V23.1 marine gravity error grid (ftp://topex.ucsd.edu/pub/global_grav_1min/; Sandwell et al. 2014) as a proxy (Figs. 8-10) to investigate possible geoid errors, but with the *caveat emptor* that we were unable to locate documentation on how this error grid was developed.

Figure 5 shows a ~150 mm difference for DTU10 MSS minus TUM13 at #6 (PSVC), which is beyond the 99% confidence bound. Figure 8 does not show a large marine gravity

anomaly error at this tide gauge, indicating an error in the DTU10MSS rather than the geoid, supported by good agreement (Fig. 5) for the AGQG2009 and EGM2008 tide gauge MDT with the ocean models at PSVC. As stated earlier, this difference has been confirmed as being attributed to an erroneous tide model used in DTU10MSS, but it offers support to the diagnostic method used here in that the difference could be correctly isolated to DTU10MSS.

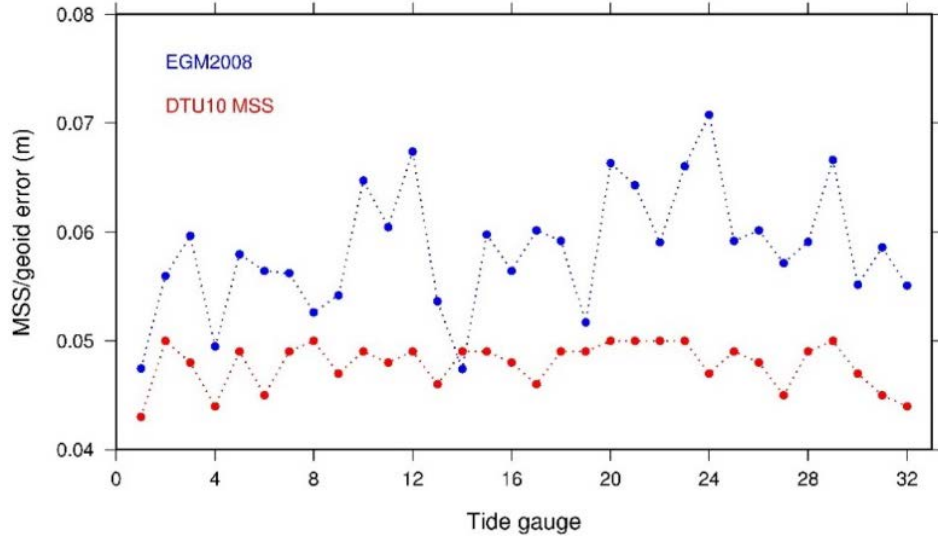


Fig. 7: Error estimates (metres) at tide gauges for DTU10MSS and EGM2008. This Fig. plotted from data downloaded from http://earth-info.nga.mil/GandG/wgs84/gravitymod/egm2008/egm08_error.html and http://www.space.dtu.dk/english/Research/Scientific_data_and_models/downloaddata

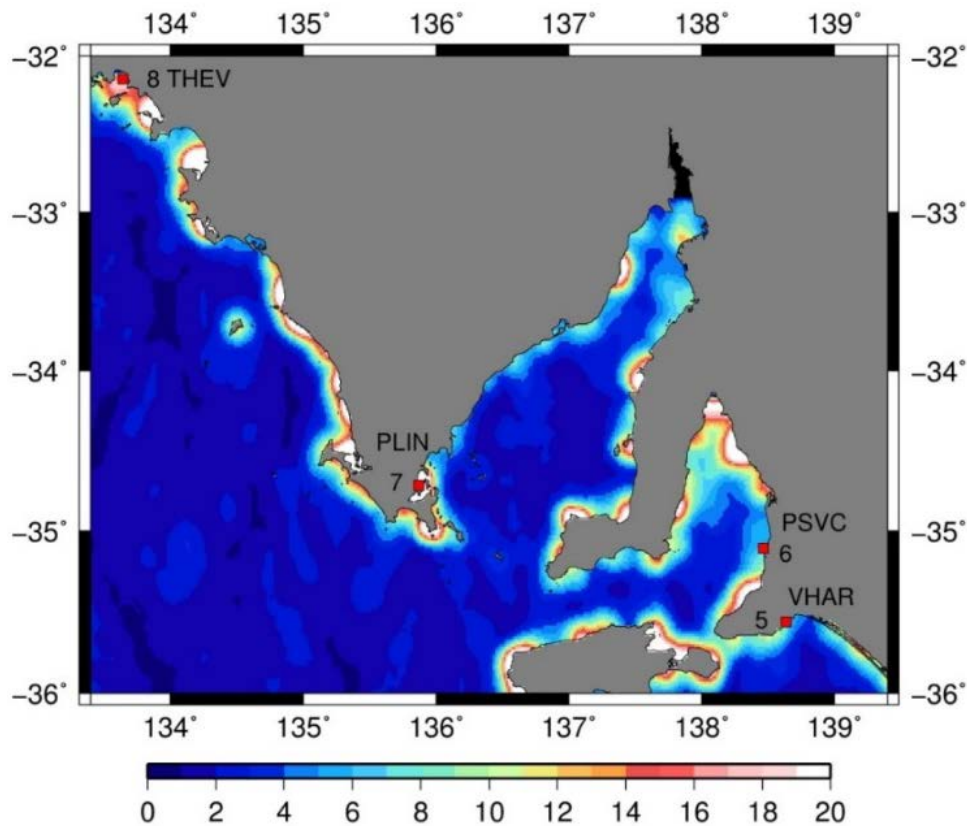


Fig. 8: Marine gravity anomaly error estimates (mGal) near selected tide gauges in southern Australia from the Sandwell V23.1 global gravity grid.

Tide gauge #7 (PLIN) shows a large difference (~ 200 mm) for all tide gauge geodetic MDTs in Fig. 5, and this does correlate with a gravity anomaly error of >20 mGal in Fig. 8, suggesting that altimetry gravity anomaly errors may have propagated into the geoid model at this location. DTU10MSS minus TUM13 indicates agreement with the ocean models, AVISO and CARS2009 (Fig. 5), again suggesting errors in the geoid models. Comparison among TUM13+EGM2008, EGM2008 and AGQG2009 indicate differences <50 mm, so we infer that DNSC08GRAV and DTU10GRAV gravity anomalies used in these geoid models may contain errors at this location.

Differences of up to ~ 200 mm are shown for tide gauge geodetic MDT at #18 (PHED) and #20 (WYND) in Fig. 5 (cf. Claessens 2012) and are outside the 99% confidence bound. Figure 9 indicates the estuarine location of WYND and gravity anomaly errors of $>\pm 20$ mGal. The WYND tide gauge is ~ 70 km from the open ocean, so that these large differences can most likely be attributed to this site not being representative of the coastal MDT. As such, it will not be investigated further and should be excluded from any attempts at VDU.

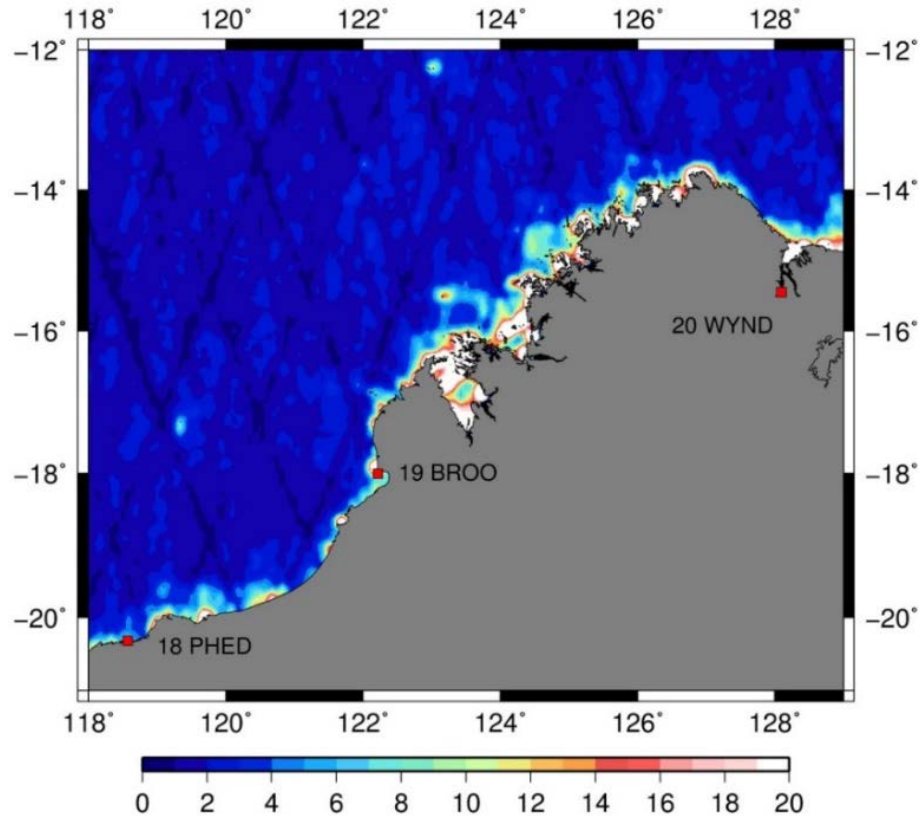


Fig. 9: Marine gravity anomaly error estimates (mGal) near selected tide gauges in the northwest of Australia from the Sandwell V23.1 global gravity grid.

PHED is slightly enigmatic, as it does not appear to be an area with large gravity anomaly errors (Fig. 9), and is also open to the ocean so that the ocean models should not be decoupled from the tide gauge location as appears to be the case for WYND. It seems oceanographically implausible that the MDT would increase 200 mm from KBAY to PHED, then back down 200 mm at BROO, as indicated by the tide gauge MSL geodetic MDT in Fig. 5. This supports the proposition of an error in the tide gauge geodetic MDT, pointing to the tide gauge levelling connection to the GNSS site, as per possible cause (3), also based on the lack of supporting evidence for a geoid error (Fig. 9). Appendix 2 shows that the PHED tide gauge is only 279 m from the GNSS site, so that the difference in geoid height should not be

large, and levelling errors should be small. The likelihood is that there may be an unidentified datum offset between the tide gauge and GNSS site, but cannot be separated from a possible geoid error without additional information, such as airborne gravity at the coast to test the short wavelength omission errors in the geoid models (e.g., McAdoo et al. 2013). Although re-levelling is preferable, this is a remote site with large surveying costs attached so that re-observation in the near future is unlikely.

On the north east coast, #26 (MACK) in Fig. 5 shows tide gauge MSL minus AGQG2009 and tide gauge MSL minus EGM2008 are beyond the 99% bound, but with tide gauge MSL minus TUM13+EGM2008 within the 99% bound. The difference between tide gauge MSL minus TUM13+EGM2008 and the other two tide gauge MSL minus MDT is ~ 100 mm. Direct comparison among these geoid models (EGM2008 is +0.036, and TUM+EGM2008 +0.117 to AGQG2009, respectively) confirms that this difference is due to the geoid models, indicating an error in EGM2008 and AGQG2009 at MACK. Marine gravity anomaly errors of ~ 10 mGal are indicated in Fig. 10 surrounding MACK, reinforcing the likelihood of geoid model error.

Figure 10 also shows marine gravity anomaly errors of ~ 20 mGal surrounding #29 (BRIS), although this appears only to manifest in the tide gauge geodetic MDT using TUM13+EGM2008, and not AGQG2009 and EGM2008. This may relate to an error in the TUM13 component of the extended TUM13+EGM2008 geoid at this site. DTU10MSS minus TUM13 does not show this large difference at BRIS, but instead agrees with AVISO. Both of these MDT are close to the 99% confidence bound, suggesting that a correlated altimetry error, and possibly coastal filtering (or simply geographical separation) has cancelled or removed the possible geoid error from the altimetric geodetic MDT. Apart from tide gauge TUM13+EGM2008, all other MDT agree within ~ 100 mm at BRIS.

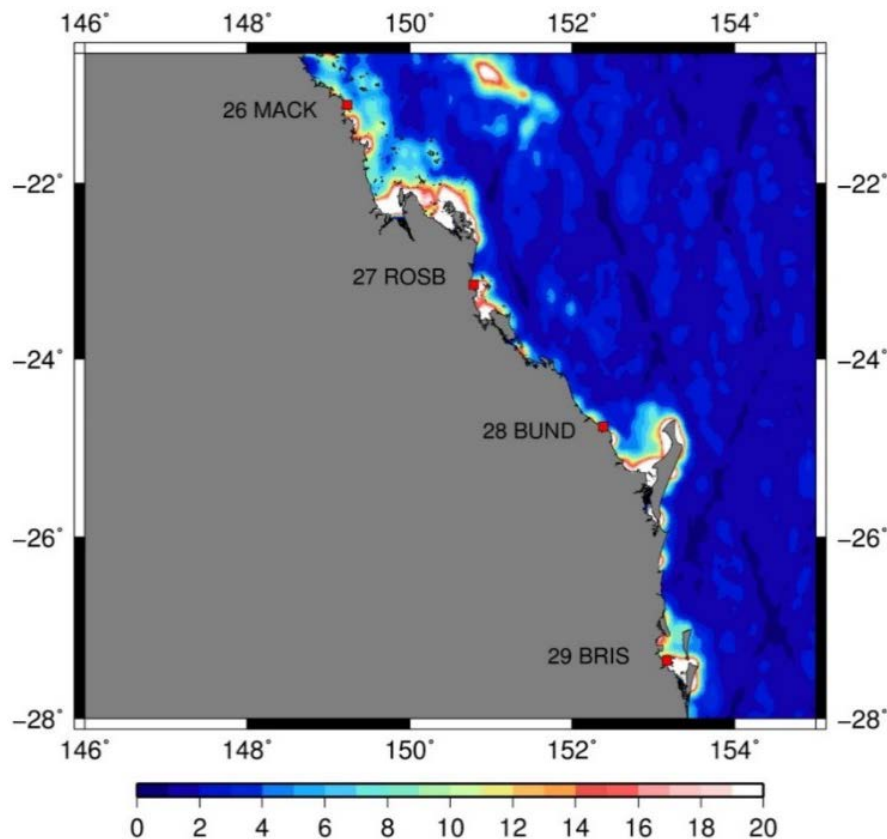


Fig. 10: Marine gravity anomaly error estimates (mGal) near selected tide gauges in the and northeast of Australia from the Sandwell V23.1 global gravity grid.

The available evidence infers that PLIN and MACK may be geoid errors (cause 2), while PHED suggests an error in the tide gauge to GNSS levelling connection (cause 3). BRIS suggests an error in TUM13 geoid at this location (cause 2, but affecting only TUM13+EGM2008). There is insufficient information for this to be conclusive however, demonstrating the need for coastal error estimates in both the ocean data and geodetic data used in the MDT models.

Finally, our values are comparable to estimates from, e.g., Ophaug et al. (2015) and Idžanović et al. (2017) along the Norwegian coast and Lin et al. (2015) along the Pacific coasts of Japan and North America. Although there may be correlation among some of the ocean models, they generally appear to provide errors of a similar magnitude, or less, than those from the geoid models at the tide gauge locations (Fig. 5). This is to say that the results for Australia appear to be representative of elsewhere, so indicative of the level of VDU achievable from geodetic and oceanographic approaches globally.

5 Comparison to levelling

As a final test of the MDT models' utility for VDU, we compare relative MDT differences with levelled height differences from the Australian National Levelling Network (ANLN) for selected tide gauge pairs (Table 4). The differences for the tide gauge pairs are computed as $\Delta H_{TG}^{lev} - \Delta H_{TG}^{MDT}$, where ΔH_{TG}^{lev} and ΔH_{TG}^{MDT} are the levelling and MDT height differences respectively between each tide gauge pair. This is a direct comparison between the levelling and MDTs, and is analogous to the analysis conducted for statistics presented in Tables 2a, 2b and 3.

This is essentially a comparison between Rummel's (2001) methods for LVD unification: (1) geodetic levelling among LVDs within one landmass, and (2) oceanographic levelling connecting tide gauges. The ANLN data were used for the realisation of the AHD, but have received updates and corrections since (e.g., Morgan 1992; Featherstone and Filmer 2012). We use a minimally constrained least-squares adjustment (MCLSA) of the ANLN, arbitrarily fixed to the single tide gauge ALBA, with normal corrections applied to the levelling observations (Filmer et al. 2010, 2014). The ANLN levelling to tide gauges refers to MSL in the period 1966-1968, so is a different epoch to the MDTs.

Tide gauge from	Tide gauge to	Distance (km)
PHED	BROO	461
CAIR	TWVL	281
BUND	BRIS	299
BRIS	PKEM	820
PLIN	THEV	352
THEV	ESPE	1113
ALBA	BUNB	280
BUNB	FREM	140
FREM	GERA	381
GERA	CARN	440
CARN	PHED	835

Table 4: Tide gauge pairs used to test MDTs with levelled height differences (see Fig 1 for locations). Geodesic distances between tide gauges were computed using the inverse method of Vincenty (1975).

The number of tide gauge pairs that can be used is limited because of (1) distortions in the ANLN resulting from systematic errors and blunders in some levelling observations (e.g., Morgan 1992; Filmer and Featherstone 2009, Featherstone and Filmer 2012, Filmer 2014),

and (2) the ANLN does not have direct levelling connections to some of the tide gauges we have used in this analysis (i.e., only local ties from the GNSS sites exist). Hence, we use tide gauge pairs in areas that are not subject by poor quality levelling data that may be misinterpreted as MDT errors. We have used mostly adjacent tide gauges, in regions where the ANLN is considered more reliable, avoiding parts of the north west, north east and central southern coasts, where the ANLN is known to contain errors.

	TUM13 (a)	AGQG (b)	TUM13+ EGM2008 (b)	CARS (c)	SODA (d1)	ECCO2 (d2)	AVISO (e)
SD	± 0.085	± 0.120	± 0.163	± 0.063	± 0.049	± 0.044	± 0.071
Max	0.138	0.099	0.271	0.088	0.029	0.069	0.060
Min	-0.150	-0.218	-0.212	-0.126	-0.112	-0.091	-0.153

Table 5: Descriptive statistics for differences between levelled height differences and MDT differences for tide gauge pairs shown in Table 4 and as defined in the text.

We use a sample of each MDT class for this comparison: DTU10 MSS minus TUM13 (a), tide gauge MSL minus AGQG2009 and TUM13+EGM2008 (b), CARS2009 (c), SODA (d1) and ECCO2 (d2), and AVISO (e). Although restricted to a relatively small sample of 11 tide gauge pairs, this provides some validation of earlier findings (and methods), with the SD of the differences indicating similar results to those in Section 3. The two ocean models shown have SD of $\sim \pm 50$ mm or less. The mean of NIOM and IOM were also computed (not shown) and had SD of ± 45 and ± 47 mm, respectively. The results in Table 5 indicate that the oceanographic MDT models (c and d) are capable of providing a better VDU than the geodetic or combined MDT models (a, b and e).

6 Conclusions

Our main aim was to compare geodetic and ocean MDTs with a view to their relative utility for VDU. The many MDT models provide a general description of the spatial variation of MDT around Australia. Most MDTs indicate large sea level gradients across northern Australia, which agree with other studies in this region. A drop of ~ 100 mm in the Gulf of Carpentaria (relative to #21 (DARW)) is shown by most ocean models, which increases by ~ 200 mm to the eastern side of the Torres Strait. These gradients are not shown by CARS2009, due to the lack of ocean information in these shallow waters.

We have inferred from combinations of the ocean and geodetic MDT data that ‘outliers’ or anomalies at five Australian tide gauges may be attributable to altimetric MSS errors (PSVC; and later confirmed as coming from a tidal model error), likely gravimetric geoid errors (PLIN, MACK and BRIS), and an uncertain connection between the tide gauge and GNSS site (PHED). However, in the absence of additional independent information, these observations cannot be considered as conclusive proof of being outliers, particularly given the inseparability of altimeter and/or geoid errors in the geodetic MDTs.

It also appears that the error grids for DTU10MSS, EGM2008 and Sandwell et al. (2014) V23.1 are optimistic in some coastal regions. Importantly, the use of independent information from the ocean-model MDTs has utility as a diagnostic for the identification of likely errors in the geodetic data. The outlier at WYND is the result of the tide gauge being located in a river, ~ 70 km from the open sea, demonstrating this site to be unsuitable for MDT studies or VDU.

To provide more evidence for the errors described, additional information such as airborne gravity over the coast would be needed to improve geoid models in these regions. An upgrade in the levelling connections from GNSS stations to tide gauges around Australia

is also required, but this is costly for remote sites. Some connections require assumptions regarding datum offsets from lowest astronomical tide to AHD at some tide gauge sites, which exacerbate the likelihood of erroneous data, given that only AHD heights are provided at the tide gauges and GNSS stations rather than the levelled height difference, which is independent of any datum offset. Additional GNSS observations with reliable ties to Australian tide gauges would also add robustness to further investigations. There are ~90 Australian RLR tide gauges listed by PSMSL (including the 32 used for this study), so there is scope for more tide gauge data for coastal MDT studies.

Our results indicate error budgets of $\sim\pm 50$ mm for some numerical ocean model MDTs (particularly SODA and ECCO2) at Australian tide gauges (Section 3), which is supported by comparisons with levelling for some tide gauge pairs (Section 5). Therefore, numerical ocean models appear a viable direct-method alternative to the geodetic boundary value or geodetic-only indirect methods for VDU (Rummel 2001). If this approach is to be taken, it would benefit from formally propagated error grids to accompany the ocean-model MDTs.

Appendix 1: Sensitivity analysis of MSL epochs

Using the 2003-2007 MSL epoch, three out of 32 tide gauge sea level records used have a one-year gap over the five-year period, but comparison of MSL values from adjacent tide gauges indicated that the missing year would cause no more than ~10 mm difference to the five-year MSL at these sites. Another consideration is that this relatively short epoch may not be representative of long-term MDT in this area, especially in the northern Australian seas where large seasonal and inter-annual differences in MSL occur (Ridgway and Godfrey 2015; Condie 2011). In addition, the inter-annual signal from ENSO (El Niño – Southern Oscillation) contributes to sea level variations (a decrease during El Niño years) at the 50-100 mm level at Australian coasts (Pariwono et al. 1986).

To test the sensitivity of tide gauge geodetic MDT to shorter time periods (cf. Coleman et al. 1979), MSL was computed for different five-year epochs; 1993-1997, 1998-2002, 2003-2007, and 2007-2011 (the latter with an overlapping year due to the data ending in 2011), and for the 19-year-long period 1993-2011. The 1993-2011 epoch was subtracted, tide gauge by tide gauge, from all five-year MSL values (Fig. A1 and Table A1). The 1993-1997 epoch shows MSL for this period below the 19-year average with the mean difference -45 mm, and largest magnitude of -93 mm for tide gauges #20 (WYND) and #22 (KARU). There is no data for #15 EXMO as this tide gauge record starts in 1998. During the 1998-2002 epoch, MSL is above the 19-year average, reaching +61 mm, but mostly around 10-20 mm. The 2007-2011 epoch is shown to be as much as +71 mm higher than the 1993-2011 MSL, with a mean difference of 40 mm. The largest differences occur across the northwest of Australia and Gulf of Carpentaria for all five-year epochs (cf. Amin, 1993; Forbes and Church, 1983; Ridgway and Godfrey 2015; Tregoning et al. 2008). On the other hand, the south eastern corner of Australia indicated differences of only ~20 mm for all five-year epochs compared to the 1993-2011 MSL.

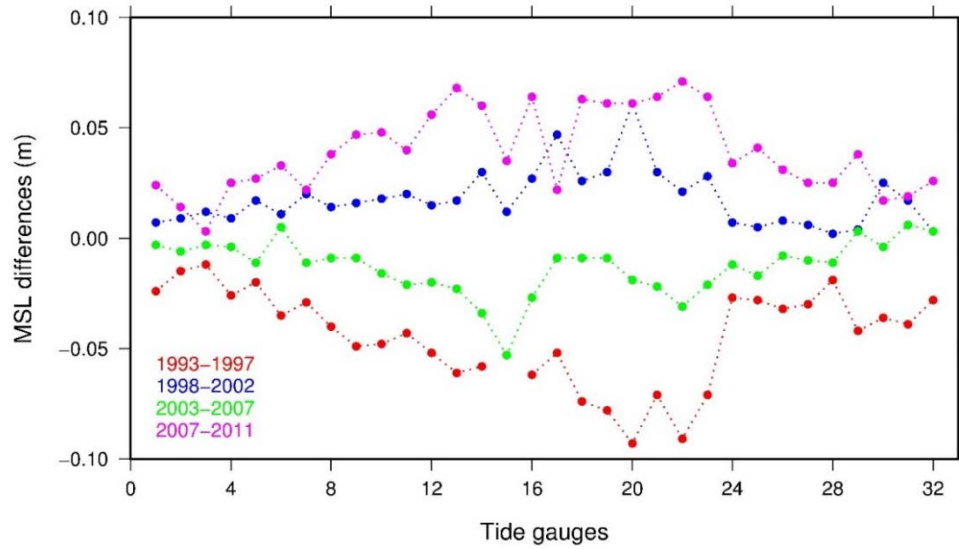


Fig. A1: Differences (metres) among five-year MSL epochs and the 19-year 1993-2011 epoch. Note that the tide gauge record for EXMO (#15) starts at 1998. Tide gauge numbers are related to tide gauge names in Fig. 1.

Epochs	SD	Max	Min	Mean
1993-1997 minus 1993-2011	± 0.022	-0.012	-0.093	-0.045
1998-2002 minus 1993-2011	± 0.013	0.061	0.002	0.018
2003-2007 minus 1993-2011	± 0.012	0.006	-0.053	-0.013
2007-2011 minus 1993-2011	± 0.019	0.071	0.003	0.040

Table A1: Descriptive statistics (metres) between tide gauge MSL over different epochs. SD, max, min and mean refer to differences in MSL over each epoch to that over 1993-2011.

In contrast, the 2003-2007 tide gauge MSL epoch does not differ by more than ~20 mm for most tide gauges (mean difference -13 mm), suggesting it is more representative of MSL over the 19 years covering 1993-2011. It is ~-30 mm at tide gauges #14 (CARN), #16 (ONSL), and #22 (KARU), reaching ~-50 mm at tide gauge #15 (EXMO), indicative of the seasonal and interannual variations of MSL in this region. It shows agreement with 1993-2011 in the Gulf of Carpentaria and Cape York. The larger difference at EXMO should be treated cautiously because the 1993-2011 average may be biased at this tide gauge because it is missing data from 1993-1997.

Appendix 2: Tide gauge and GNSS information

#	TG	TG Name	PSMSL 680 STN #	TG Lon	TG Lat	Years (gaps)	TG to GNSS (m)	GNSS h ITRF2008 @2005.5 (m)	GNSS h Standard deviation (mm)
1	BURN	Burnie	193	145.914993	-41.050083	1993-2011	12	3.061	0.1
2	STON	Stony Point	178	145.224701	-38.372139	1993-2011	207	6.281	0.45
3	LORN	Lorne	226	143.988831	-38.547195	1993-2011(1)	234	5.087	0.49
4	PORT	Portland	231	141.613174	-38.343445	1993-2011	965	-1.592	0.54
5	VHAR	Victor Harbor	275	138.635406	-35.562481	1993-2011(2)	125	2.284	0.49
6	PSVC	Port Stanvac	298	138.467026	-35.108612	1993-2010(1)	1285	48.611	0.44
7	PLIN	Port Lincoln	431	135.870010	-34.715904	1993-2011	455	-2.434	0.41
8	THEV	Thevenard	441	133.641327	-32.148945	1993-2011	566	5.956	0.46
9	ESPE	Esperance	446	121.895363	-33.870888	1993-2011	374	28.782	22.96
10	ALBA	Albany	451	117.892555	-35.033722	1993-2011	157	-28.648	0.43
11	BUNB	Bunbury	461	115.659973	-33.323444	1993-2011(1)	1303	-30.584	0.34
12	FREM	Fremantle	471	115.748138	-32.065556	1993-2011	1362	-29.119	10.0*
13	GERA	Geraldton	474	114.601891	-28.775972	1993-2011	39	-23.192	0.46
14	CARN	Carnarvon	479	113.651031	-24.898693	1993-2011	3238	-12.759	2.03
15	EXMO	Exmouth	482	114.140892	-21.954861	1998-2011	4215	0.400	1.29
16	ONSL	Onslow	483	115.131531	-21.649668	1993-2011	2911	8.308	5.02
17	KBAY	King Bay	486	116.749054	-20.623611	1993-2010(1)	544	10.389	2.76
18	PHED	Port Hedland	494	118.574417	-20.317583	1993-2011	279	3.502	14.0*
19	BROO	Broome	497	122.218636	-18.000834	1993-2011	1069	42.236	16.0*
20	WYND	Wyndham	507	128.101028	-15.453278	1993-2011(1)	664	43.278	0.47
21	DARW	Darwin	011	130.845856	-12.471778	1993-2011	762	80.307	0.81
22	KARU	Karumba	018	140.833328	-17.500000	1993-2011(4)	1186	55.965	0.21
23	WEIP	Weipa	021	141.866669	-12.666667	1993-2011	2829	78.285	0.49
24	CAIR	Cairns	041	145.783340	-16.916668	1993-2011	2204	65.486	0.57
25	TWVL	Townsville I	051	146.833328	-19.250000	1993-2011	378	62.400	0.43
26	MACK	Mackay	061	149.233337	-21.100000	1993-2011	1435	64.377	0.43
27	ROSB	Roslyn Bay	069	150.790161	-23.161028	1994-2011	391	59.328	0.46
28	BUND	Bundaberg	073	152.383331	-24.766666	1993-2011	536	52.081	0.53

29	BRIS	Brisbane	078	153.166672	-27.366667	1993-2011	5071	49.426	0.38
30	NEWC	Newcastle V	135	151.788589	-32.924000	1993-2011	1085	54.425	2.43
31	PKEM	Port Kembla	161	150.911865	-34.473751	1993-2011	90	24.743	0.46
32	SBAY	Spring Bay	199	147.932724	-42.545860	1993-2011	169	-0.968	0.12

Table A2: Australian tide gauge records for 1993 – 2011, which corresponds approximately with the availability of satellite altimetry data. Gaps in records (years) are indicated in parenthesis. Data from PSMSL (<http://www.psmsl.org/data/obtaining/>; Holgate et al. 2013). Distance (to the nearest meter) from tide gauge to GNSS location computed using Vincenty’s inverse solution (Vincenty 1975). GNSS h and standard deviations are from the processed BERN output (Hu 2009). The standard deviations should be scaled by 10 to provide more realistic error estimates (Rothacher 2002). Three stations marked * were processed using AUSPOS from data provided by Landgate. The standard deviations from these processed heights are at 95% confidence.

Acknowledgements

Chris Hughes and Rory Bingham were funded by ESA via the project ITT AO/1-8194/15/NL/FF/gp “GOCE++ Dynamic Topography at the coast and tide gauge unification”. Part of this work was funded by UK Natural Environment Research Council National Capability funding. Thanks to Jack McCubbine for discussion on coastal geoid errors. We would like to thank the following agencies and organisations for allowing access to data: Geoscience Australia (GNSS at tide gauges available on request from Nick Brown Nicholas.Brown@ga.gov.au); PSMSL, CSIRO for CARS2009, AVISO; Technical University of Denmark (DTU) for DTU10 MSS, Technical University of Munich for TUM2013, National Geospatial-Intelligence Agency (NGA) EGM Development Team for EGM2008, Scripps Institution of Oceanography (University of California) for V23.1 marine gravity error grid (data from SIO, NOAA and NGS) and the bathymetry data used in Fig. 1. Figures 1-10 and Fig. A1 were plotted using the Generic Mapping Tools (Wessel et al. 2013). We appreciate comments from Associate Editor Benoit Meyssignac, and three anonymous reviewers that have helped us to improve this manuscript.

References

- Altamimi Z, Collilieux X, Legrand J, Garayt B, Boucher C (2007) ITRF2005: A new release of the International Terrestrial Reference Frame based on time series of station positions and Earth Orientation Parameters. *J Geophys Res Solid Earth* 112:B09401. <https://doi.org/10.1029/2007JB004949>.
- Altamimi Z, Collilieux X, Métivier L (2011) ITRF2008: An improved solution of the International Terrestrial Reference Frame. *J Geod* 85(8):457–473. <https://doi.org/10.1007/s00190-011-0444-4>.
- Amin M (1988) Spatial variations of mean sea level of the North Sea off the east coast of Britain. *Cont Shelf Res* 8:1087–1106. [https://doi.org/10.1016/0278-4343\(88\)90040-4](https://doi.org/10.1016/0278-4343(88)90040-4).
- Amin M (1993) Changing mean sea level and tidal constants on the west coast of Australia. *Aust J Mar Freshwater Res* 44(6):911–925. <https://doi.org/10.1071/MF9930911>.
- Amjadiparvar B, Rangelova E, Sideris MG (2016) The GBVP approach for vertical datum unification: recent results in North America. *J Geod* 90:45–63. <https://doi.org/10.1007/s00190-015-0855-8>.
- Amos MJ, Featherstone WE (2009) Unification of New Zealand’s local vertical datums: iterative gravimetric quasigeoid computations. *J Geod* 83:57–68. <https://doi.org/10.1007/s00190-008-0232-y>.
- Andersen OB (1999) Shallow water tides in the northwest European shelf region from TOPEX/POSEIDON altimetry. *J Geophys Res* 104(C4):7729–7741. <https://doi.org/10.1029/1998JC900112>.
- Andersen OB, Knudsen P, Berry PAM (2010) The DNSC08GRA global marine gravity field from double retracked satellite altimetry. *J Geod* 84(3):191–199. <https://doi.org/10.1007/s00190-009-0355-9>.
- Andersen OB, Knudsen P (2009) DNSC08 mean sea surface and mean dynamic topography models. *J Geophys Res Oceans* 114:C11001. <https://doi.org/10.1029/2008JC005179>.
- Arabelos D, Tscherning CC (2001) Improvements in height datum transfer expected from the GOCE mission. *J Geod* 75(5-6):308–312. <https://doi.org/10.1007/s001900100187>.
- Ardalan AA, Safari A (2005) Global height datum unification: a new approach in gravity potential space. *J Geod* 79(9):512–523. <https://doi.org/10.1007/s00190-005-0001-0>.
- Balasubramania N (1994) Definition and realization of a global vertical datum. Report 427, The Ohio State University, Columbus, USA.
- Bingham RJ, Hughes CW (2012) Local diagnostics to estimate density-induced sea level variations over topography and along coastlines. *J Geophys Res Oceans* 117:C01013. <https://doi.org/10.1029/2011JC007276>.
- Bingham RJ, Haines K, Hughes CW (2008) Calculating the ocean’s mean dynamic topography from a mean sea surface and a geoid. *J Atmos Ocean Tech* 25(10):1808–1822. <https://doi.org/10.1175/2008JTECHO568.1>.
- Bingham RJ, Haines K, Lea DJ (2014) How well can we measure the ocean’s mean dynamic topography from space? *J Geophys Res Oceans* 119(6):3336–3356. <https://doi.org/10.1002/2013JC009354>.
- Blaker AT, Hirschi JJ-M, McCarthy G, Sinha B, Taws S, Marsh R, Coward A, de Cuevas B (2014) Historical analogues of the recent extreme minima observed in the Atlantic meridional overturning circulation at 26°N. *Clim Dyn* 44(1-2):457–473. <https://doi.org/10.1007/s00382-014-2274-6>.
- Bolkas D, Fotopoulos G, Sideris MG (2012) Referencing regional geoid-based vertical datums to national tide gauge networks. *J Geod Sci* 2(4):363–369. <https://doi.org/10.2478/v10156-011-0050-7>.
- Bruinsma SL, Foerste C, Abrikosov O, Marty JC, Rio M-H, Mulet S, Bonvalot S (2013) The new ESA satellite-only gravity field model via the direct approach. *Geophys Res Lett* 40:3607–3612. <https://doi.org/10.1002/grl.50716>.

- Carton JA, Giese BS (2008) A reanalysis of ocean climate using Simple Ocean Data Assimilation (SODA). *Mon Weather Rev* 136:2999-3017. <https://doi.org/10.1175/2007MWR1978.1>.
- Cartwright DE, Crease J (1963) A comparison of the geodetic reference levels of England and France by means of the sea surface. *Proc Royal Soc Lon A* 273:558-580. <https://doi.org/10.1098/rspa.1963.0109>.
- Chang YS, Zhang S, Rosati A, Delworth TL, Stern WF (2013) An assessment of oceanic variability for 1960–2010 from the GFDL ensemble coupled data assimilation. *Clim Dyn* 40(3-4):775-803. <https://doi.org/10.1007/s00382-012-1412-2>.
- Christie RR (1994) A new geodetic heighting strategy for Great Britain. *Surv Rev* 32(252):328-343. <https://doi.org/10.1179/sre.1994.32.252.328>.
- Claessens SJ (2012) Evaluation of gravity and altimetry data in Australian coastal regions. In *Geodesy for Planet Earth*, Proc. IAG Symposium 136, edited by Kenyon et al., pp. 435-442. https://doi.org/10.1007/978-3-642-20338-1_52.
- Coleman R, Rizos C, Masters EG, Hirsch B (1979) The investigation of the sea surface slope along the north eastern coast of Australia. *Aust J Geod Photo Surv* 31:686-699.
- Colombo OL (1980) A world vertical network. Report 296, The Ohio State University, Columbus, USA.
- Condie SA (2011) Modeling seasonal circulation, upwelling and tidal mixing in the Arafura and Timor Seas. *Cont Shelf Res* 31(14):1427-1436. <https://doi.org/10.1016/j.csr.2011.06.005>.
- Cummings JA, Smedstad OM (2013) Variational Data Assimilation for the Global Ocean. In *Data Assimilation for Atmospheric, Oceanic and Hydrologic Applications - II*, edited by SK Park and L Xu, pp. 303-343. https://doi.org/10.1007/978-3-642-35088-7_13.
- Deng XL, Featherstone WE, Hwang C (2002) Estimation of contamination of ERS-2 and POSEIDON satellite radar altimetry close to the coasts of Australia. *Mar Geod* 25(4):249-271. <https://doi.org/10.1080/01490410290051572>.
- Drinkwater MR, Floberghagen R, Haagmans R, Muzi D, Popescu A (2003) GOCE: ESA's first Earth Explorer Core mission. In *Earth Gravity Field from Space - from Sensors to Earth Sciences*, edited by G. Beutler et al., pp. 419–432, Springer, Dordrecht, Netherlands. https://doi.org/10.1007/978-94-017-1333-7_36.
- Dunn J, Ridgway KR (2002) Mapping ocean properties in regions of complex topography. *Deep Sea Res - I* 49(3):591-604. [https://doi.org/10.1016/S0967-0637\(01\)00069-3](https://doi.org/10.1016/S0967-0637(01)00069-3).
- Ekman M (1989) Impacts of geodynamic phenomena on systems for height and gravity. *Bull Géod* 63(3):281-296. <https://doi.org/10.1007/BF02520477>.
- Featherstone WE, Filmer MS (2012) The north-south tilt in the Australian Height Datum is explained by the ocean's mean dynamic topography. *J Geophys Res* 117:C08035. <https://doi.org/10.1029/2012JC007974>.
- Featherstone WE, Kirby JF, Hirt C, Filmer MS, Claessens SJ, Brown NJ, Hu G, Johnston GM (2011) The AUSGeoid09 model of the Australian Height Datum. *J Geod* 85(3):133-150. <https://doi.org/10.1007/s00190-010-0422-2>.
- Fecher T, Pail R, Gruber T (2015) Global gravity field modeling based on GOCE and complementary gravity data. *Int J Appl Earth Obs Geoinf* 35(A):120–127. <https://doi.org/10.1016/j.jag.2013.10.005>.
- Ferry N, Parent L, Garric G, Bricaud C, Testut C-E, Le Galloudec O, Lellouche J-M, Drevillon M, Greiner E, Barnier B, Molines J-M, Jourdain NC, Guinehut S, Cabanes C, Zawadzki L (2012) GLORYS2V1 global ocean reanalysis of the altimetric era (1992-2009) at meso-scale. *Mercator Ocean Quarterly Newsletter* 44:29-39.
- Filmer MS (2014) Using models of the ocean's mean dynamic topography to identify errors in coastal geodetic levelling. *Mar Geod* 37(1):47–64. <https://doi.org/10.1080/01490419.2013.868383>.
- Filmer MS, Featherstone WE (2009) Detecting spirit-levelling errors in the AHD: recent findings and some issues for any new Australian height datum. *Aust J Earth Sci* 56(4):559–569. <https://doi.org/10.1080/08120090902806305>.
- Filmer MS, Featherstone WE (2012) A re-evaluation of the offset in the Australian Height Datum between mainland Australia and Tasmania. *Mar Geod* 35(1):107-119. <https://doi.org/10.1080/01490419.2011.634961>.
- Filmer MS, Featherstone WE, Kuhn M (2010) The effect of EGM2008-based normal, normal-orthometric and Helmert orthometric height systems on the Australian levelling network. *J Geod* 84(8):501–513. <https://doi.org/10.1007/s00190-010-0388-0>.
- Filmer MS, Featherstone WE, Kuhn M (2014) Erratum to: The effect of EGM2008-based normal, normal-orthometric and Helmert orthometric height systems on the Australian levelling network. *J Geod* 88(1):93. <https://doi.org/10.1007/s00190-013-0666-8>.
- Filmer MS, Featherstone WE, Claessens SJ (2014) Variance component estimation uncertainty for unbalanced data: application to a continent-wide vertical datum. *J Geod* 88(11):1081-1093. <https://doi.org/10.1007/s00190-014-0744-6>.
- Forbes AMG, Church JA (1983) Circulation in the Gulf of Carpentaria II: residual currents and mean sea level. *Aust J Mar Freshw Res* 34(1):11–22. <https://doi.org/10.1071/MF9830011>.

- Forget G, Campin J-M, Heimbach P, Hill CN, Ponte RM, Wunsch C (2015) ECCO version 4: an integrated framework for non-linear inverse modeling and global ocean state estimation. *Geosci Model Dev* 8:3071–3104. <https://doi.org/10.5194/gmd-8-3071-2015>.
- Ganachaud A, Wunsch C, Kim M-C, Tapley B (1997) Combination of TOPEX/POSEIDON data with a hydrographic inversion for determination of the oceanic general circulation and its relation to geoid accuracy. *Geophys J Int* 128(3):708–722. <https://doi.org/10.1111/j.1365-246X.1997.tb05331.x>.
- Gerlach C, Rummel R (2013) Global height system unification with GOCE: a simulation study on the indirect bias term in the GBVP approach. *J Geod* 87(1):57–67. <https://doi.org/10.1007/s00190-012-0579-y>.
- Grombein T, Seitz K, Heck B (2017) On high-frequency topography-implied gravity signals for a height system unification using GOCE-based global geopotential models. *Surv Geophys* 38:443–477. <https://doi.org/10.1007/s10712-016-9400-4>.
- Gruber T, Gerlach C, Haagmans R (2012) Intercontinental height datum connection with GOCE and GPS-levelling data. *J Geod Sci* 2(4):270–280. <https://doi.org/0.2478/v10156-012-0001-y>.
- Hamon BV, Greig MA (1972) Mean sea level in relation to geodetic land leveling around Australia. *J Geophys Res* 77(36):7157–7162. <https://doi.org/10.1029/JC077i036p07157>.
- Higginson S, Thompson KR, Woodworth PL, Hughes CW (2015) The tilt of mean sea level along the east coast of North America. *Geophys Res Lett* 42(5):1471–1479. <https://doi.org/10.1002/2015GL063186>.
- Hipkin RG (2000) Modelling the geoid and sea-surface topography in coastal areas. *Phys Chem Earth - Part A* 25(1):9–16. [https://doi.org/10.1016/S1464-1895\(00\)00003-X](https://doi.org/10.1016/S1464-1895(00)00003-X).
- Holgate SJ, Matthews A, Woodworth PL, Rickards LJ, Tamisiea ME, Bradshaw E, Foden PR, Gordon KM, Jerejeva S, Pugh J (2013) New data systems and products at the Permanent Service for Mean Sea Level. *J Coast Res* 29(3):493–504. <https://doi.org/10.2112/JCOASTRES-D-12-00175.1>.
- Hughes CW, Bingham RJ, Roussenov V, Williams J, Woodworth PL (2015) The effect of Mediterranean exchange flow on European time-mean sea level. *Geophys Res Lett* 42(2):466–474. <https://doi.org/10.1002/2014GL062654>.
- Hu G R (2009) Analysis of regional GPS campaigns and their alignment to the International Terrestrial Reference Frame (ITRF). *J Spat Sci* 54(1):15–22. <https://doi.org/10.1080/14498596.2009.9635163>.
- Huang J (2017) Determining coastal mean dynamic topography by geodetic methods. *Geophys Res Lett* 44(21):11125–11128. <https://doi.org/10.1002/2017GL076020>.
- Idris NH, Deng X, Andersen OB (2014) The importance of coastal altimetry retracking and detiding: a case study around the Great Barrier Reef, Australia. *Int J Rem Sens* 35(5):1729–1740. <https://doi.org/10.1080/01431161.2014.882032>.
- Idžanović M, Ophaug V, Andersen OB (2017) The coastal mean dynamic topography in Norway observed by CryoSat-2 and GOCE. *Geophys Res Lett* 44(11):5609–5617. <https://doi.org/10.1002/2017GL073777>.
- Jayne SR (2006) Circulation of the North Atlantic Ocean from altimetry and the Gravity Recovery and Climate Experiment geoid. *J Geophys Res Oceans* 111(C3):C03005. <https://doi.org/10.1029/2005JC003128>.
- Kistler R, Collins W, Saha S, White G, Woollen J, Kalnay E, Chelliah M, Ebisuzaki W, Kanamitsu M, Kousky V, van den Dool H, Jenne R, Fiorino M (2001) The NCEP-NCAR 50 year reanalysis: Monthly means CD-ROM and documentation. *Bull Am Meteorol Soc* 82:247–267. [https://doi.org/10.1175/1520-0477\(2001\)082<0247:TNNYRM>2.3.CO;2](https://doi.org/10.1175/1520-0477(2001)082<0247:TNNYRM>2.3.CO;2).
- Knudsen P, Bingham RJ, Andersen OB, Rio M-H (2011) A global mean dynamic topography and ocean circulation estimation using a preliminary GOCE gravity model. *J Geod* 85(11):861–879. <https://doi.org/10.1007/s00190-011-0485-8>.
- Köhl A, Stammer D, Cornuelle B (2007) Interannual to decadal changes in the ECCO global synthesis. *J Phys Oceanogr* 37:313–337. <https://doi.org/10.1175/JPO3014.1>.
- Lin H, Thompson KR, Huang J, Véronneau M (2015) Tilt of mean sea level along the Pacific Coasts of North America and Japan. *J Geophys Res Oceans* 120(10): 6815–6828. <https://doi.org/10.1002/2015JC010920>.
- Losch M, Sloyan SM, Schröter J, Sneeuw N (2002) Box inverse models, altimetry and the geoid: Problems with the omission error. *J Geophys Res Oceans* 107(C7):3078. <https://doi.org/10.1029/2001JC000855>.
- Marshall J, Hill C, Perelman L, Adcroft A (1997a) Hydrostatic, quasi-hydrostatic, and ocean modeling. *J Geophys Res Oceans* 102(C3):5733–5752. <https://doi.org/10.1029/96JC02776>.
- Marshall J, Adcroft A, Hill C, Perelman L, Heisey C (1997b) A finite-volume, incompressible Navier Stokes model for studies of the ocean on parallel computers. *J Geophys Res* 102(C3):5753–5766. <https://doi.org/10.1029/96JC02775>.
- Maximenko NA, Niiler P, Rio M-H, Melnichenko O, Centurioni L, Chambers D, Zlotnicki V, Galepin B (2009) Mean dynamic topography of the ocean derived from satellite and drifting buoy data using three different techniques. *J Atmos Oceanic Technol* 26:1910–1919. <https://doi.org/10.1175/2009JTECHO672.1>.
- Mazloff, MR, Gille ST, Cornuelle B (2014) Improving the geoid: Combining topography in the California coastal ocean. *Geophys Res Lett* 41(24):8944–8952. <https://doi.org/10.1002/2014GL062402>.

- McAdoo DC, Farrell SL, Laxon S, Ridout A, Zwally HJ, Yi D (2013) Gravity of the Arctic Ocean from satellite data with validations using airborne gravimetry: Oceanographic implications. *J Geophys Res Oceans* 118(2):917–930. <https://doi.org/10.1002/jgrc.20080>.
- Menemenlis D, Fukumori I, Lee T (2005) Using Green's functions to calibrate an ocean general circulation model. *Mon Weather Rev* 133:1224–1240. <https://doi.org/10.1175/MWR2912.1>.
- Menemenlis D, Wunsch C (1997) Linearization of an oceanic circulation model for data assimilation and climate studies. *J Atmos Oceanic Technol* 14(6):1420–1443. [https://doi.org/10.1175/1520-0426\(1997\)014<1420:LOAOGC>2.0.CO;2](https://doi.org/10.1175/1520-0426(1997)014<1420:LOAOGC>2.0.CO;2).
- Mitchell HL (1975) Sea-surface topography around Australia. *Surv Geophys* 2(1):117–129. <https://doi.org/10.1007/BF01447940>.
- Morgan P (1992) An analysis of the Australian Height Datum: 1971. *Aust Surv* 37(1):46–63. <https://doi.org/10.1080/00050326.1992.10438774>.
- Ophaug V, Breili K, Gerlach C (2015) A comparative assessment of coastal mean dynamic topography in Norway by geodetic and ocean approaches. *J Geophys Res* 120(12):7807–7826. <https://doi.org/10.1002/2015JC011145>.
- Pariwono JI, Bye JAT, Lennon GW (1986) Long period variations in sea level in Australasia. *Geophys J R Astr Soc* 87(1):43–54. <https://doi.org/10.1111/j.1365-246X.1986.tb04545.x>.
- Pavlis NK, Holmes SA, Kenyon SC, Factor JF (2012) The development and evaluation of Earth Gravitational Model (EGM2008). *J Geophys Res Solid Earth* 117(B4):B04406. <https://doi.org/10.1029/2011JB008916>.
- Pavlis NK, Holmes SA, Kenyon SC, Factor JK (2013) Correction to “The development and evaluation of the Earth Gravitational Model 2008 (EGM2008)”. *J Geophys Res* 118(B5): 2633. <https://doi.org/10.1029/jgrb.50167>.
- Pavlis NK, Saleh J (2005) Error propagation with geographic specificity for very high degree geopotential models. In *Gravity, Geoid and Space Missions, IAG Symposia- 129* edited by C. Jekeli et al., pp 149–154, https://doi.org/10.1007/3-540-26932-0_26.
- Penna NT, Featherstone WE, Gazeaux J, Bingham RJ (2013) The apparent British sea slope is caused by systematic errors in the levelling based vertical datum. *Geophys J Int* 194(2):772–786. <https://doi.org/10.1093/gji/ggt161>
- Petit G, Luzum B (eds.) (2010) *IERS conventions 2010* (IERS Technical Note No. 36), Frankfurt am Main, pp. 179.
- Rapp RH (1994) Separation between reference surfaces of selected vertical datums. *Bull Géod* 69(1):26–31. <https://doi.org/10.1007/BF00807989>.
- Rapp RH, Balasubramania N (1992) A conceptual formulation of a world height system. Report 421, Department of Geodetic Science and Surveying, Ohio State University, USA.
- Ridgway KR (2007) Long-term trend and decadal variability of the southward penetration of the East Australia Current. *Geophys Res Lett* 34(13):L13613. <https://doi.org/10.1029/2007GLO30393>.
- Ridgway KR, Condie SA (2004) The 5,500-km long boundary flow off western and southern Australia. *J Geophys Res Oceans* 109(C4):C04017. <https://doi.org/10.1029/2003JC001921>.
- Ridgway KR, Godfrey JS (2015) The source of the Leeuwin Current seasonality. *J Geophys Res* 120(10):6843–6864. <https://doi.org/10.1002/2015JC011049>.
- Ridgway KR, Dunn JR, Wilkin JL (2002) Ocean interpolation by four-dimensional weighted least squares-application to the waters around Australasia. *J Atmos Ocean Tech* 19(9):1357–1375. [https://doi.org/10.1175/1520-0426\(2002\)019<1357:OIBFDW>2.0.CO;2](https://doi.org/10.1175/1520-0426(2002)019<1357:OIBFDW>2.0.CO;2)
- Ridgway KR, Dunn JR (2003) Mesoscale structure of the mean East Australian Current system and its relationship with topography. *Prog Oceanog* 56(2):189–222. [https://doi.org/10.1016/S0079-6611\(03\)00004-1](https://doi.org/10.1016/S0079-6611(03)00004-1).
- Rio M-H, Hernandez F (2004) A mean dynamic topography computed over the world ocean from altimetry, in-situ measurements and a geoid model. *J Geophys Res Oceans* 109(C12):C12032. <https://doi.org/10.1029/2003JC002226>.
- Rio M-H, Guinehut S, Larnicol G (2011) The New CNES-CLS09 global Mean Dynamic Topography computed from the combination of GRACE data, altimetry and in-situ measurements. *J Geophys Res* 116(C7):C07018. <https://doi.org/10.1029/2010JC006505>.
- Rio M-H, Mulet S, Picot N (2014) Beyond GOCE for the ocean circulation estimate: Synergetic use of altimetry, gravimetry, and in situ data provides new insight into geostrophic and Ekman currents. *Geophys Res Lett* 41(24):8918–8925. <https://doi.org/10.1002/2014GL061773>.
- Roelse A, Granger HW, Graham JW (1971, 2nd edn. 1975) *The adjustment of the Australian levelling survey 1970–1971*. Technical Report 12. Division of National Mapping, Canberra.
- Rothacher M (2002) Estimation of station heights with GPS, in *Vertical Reference Systems*, edited by H. Drewes et al., pp. 81–90, Springer, Berlin. https://doi.org/10.1007/978-3-662-04683-8_17.

- Rummel R (2001) Global unification of height systems and GOCE. In: Sideris MG (ed.) Gravity, geoid and geodynamics 2000. pp 13–20, Springer, Berlin. https://doi.org/10.1007/978-3-662-04827-6_3.
- Rummel R, Teunissen P (1988). Height datum definition, height datum connection and the role of the geodetic boundary value problem. *Bull Géod* 62(4):477-498. <https://doi.org/10.1007/BF02520239>.
- Rummel R, Ilk KH (1995) Height datum connection-the ocean part. *Allgemeine Vermessungsnachrichten* 8–9:321–330.
- Sánchez L, Čunderlík R, Dayoub N, Mikula K, Minarechová Z, Šíma Z, Vátr V, Vojtíšková M (2016) A conventional value for the geoid reference potential W_0 . *J Geod* 90(9):815-835. <https://doi.org/10.1007/s00190-016-0913-x>.
- Sandwell DT, Müller RD, Smith WHF, Garcia E, Francis R (2014) New global marine gravity model from CryoSat-2 and Jason-1 reveals buried tectonic structure. *Science* 346(6205):65-67, <https://doi.org/10.1126/science.1258213>.
- Schaeffer P, Faugère Y, Legeais JF, Ollivier A, Guinle T, Picot N (2012) The CNES_CLS11 global mean sea surface computed from 16 years of satellite altimeter data. *Mar Geod* 35(1):3–19. <https://doi.org/10.1080/01490419.2012.718231>.
- Slobbe DC, Klees R (2014) The impact of the dynamic sea surface topography on the quasi-geoid in shallow coastal waters. *J Geod* 88(3):241–261. <https://doi.org/10.1007/s00190-013-0679-3>.
- Smith WHF, Sandwell DT (1997) Global seafloor topography from satellite altimetry and ship depth soundings. *Science* 277(5334):1957-1962. <https://doi.org/10.1126/science.277.5334.1956>
- Smith WHF, P. Wessel (1990) Gridding with continuous curvature splines in tension. *Geophys* 55(3):293-305. <https://doi.org/10.1190/1.1442837>.
- Soufflet Y, Marchesiello P, Lemarié F, Jouanno J, Capet X, Debreu L, Benshila R (2016) On effective resolution in ocean models. *Ocean Modelling* 98:36-50. <https://doi.org/10.1016/j.ocemod.2015.12.004>.
- Tapley BD, Bettadpur S, Watkins M, Reigber C (2004) The gravity recovery and climate experiment: Mission overview and early results. *Geophys Res Lett* 31:L09607, <https://doi.org/10.1029/2004GL019920>.
- Teunissen PJG, Amiri-Simkooei A (2008) Least-squares variance component estimation. *J Geod* 82(2):65–82. <https://doi.org/10.1007/s00190-007-0157>.
- Tregoning P, Lambeck K, Ramillien G (2008) GRACE estimates of sea surface height anomalies in the Gulf of Carpentaria, Australia. *Earth Plan Sci Lett* 271(1-4):241-244. <https://doi.org/10.1016/j.epsl.2008.04.018>.
- Valdivieso M, Haines K, Zuo H, Lea D (2014) Freshwater and heat transports from global ocean synthesis. *J Geophys Res* 119(1):394–409. <https://doi.org/10.1002/2013JC009357>.
- Vignudelli S, Kostianoy A, Cipollini P, Benveniste J (eds) (2011) Coastal altimetry. Springer, Berlin, p. 566. <https://doi.org/10.1007/978-3-642-12796-0>.
- Vincenty T (1975) Direct and inverse solutions of geodesics on the ellipsoid with application of nested equations. *Surv Rev* 23(176):88-93. <https://doi.org/10.1179/sre.1975.23.176.88>.
- Vinogradov SV, Ponte RM (2011) Low-frequency variability in coastal sea level from tide gauges and altimetry. *J Geophys Res Oceans* 116(C7):C07006. <https://doi.org/10.1029/2011JC007034>.
- Volkov DL, Larnicol G, Dorandeu J (2007) Improving the quality of satellite altimetry data over continental shelves. *J Geophys Res Oceans* 112(C6):C06020. <https://doi.org/10.1029/2006JC003765>.
- Vossepoul FC (2007) Uncertainties in the mean ocean dynamic topography before the launch of the Gravity Field and Steady-State Ocean Circulation Explorer (GOCE). *J Geophys Res Oceans* 112(C5):C05010. <https://doi.org/10.1029/2006JC003891>.
- Wessel P, Smith WHF, Scharroo R, Luis JF, Wobbe F (2013) Generic Mapping Tools: Improved version released. *EOS - Trans AGU*, 94(45):409-410. <https://doi.org/10.1002/2013EO450001>.
- Williams RG, Roussenov V, Smith D, Lozier MS (2014) Decadal evolution of ocean thermal anomalies in the North Atlantic: The effects of Ekman, overturning, and horizontal transport. *J Clim* 27:698–719, <https://doi.org/10.1175/JCLI-D-12-00234.1>.
- Wolanski E, Lambrechts J, Thomas C, Deleersnijder E (2013) The net water circulation through Torres Strait. *Cont Shelf Res* 64:66-74, <https://doi.org/10.1016/j.csr.2013.05.013>.
- Woodworth PL (2012) A note on the nodal tide in sea level records. *J Coastal Res* 28(2):316-323, <https://doi.org/10.2112/JCOASTRES-D-11A-00023.1>.
- Woodworth PL, Hughes CW, Bingham RW, Gruber T (2012) Towards worldwide height system unification using ocean information. *J Geod Sci* 2(4):302–318. <https://doi.org/10.2478/v10156-012-004-8>.
- Woodworth PL, Gravelle M, Marcos M, Wöppelmann G, Hughes CW (2015) The status of measurement of the Mediterranean mean dynamic topography by geodetic techniques. *J Geod* 89(8):811–827. <https://doi.org/10.1007/s00190-015-0817-1>
- Wunsch C (1978) The North Atlantic general circulation west of 50°W determined by inverse methods. *Rev Geophys Space Phys* 16(4):583-620. <https://doi.org/10.1029/RG016i004p00583>.
- Wunsch C, Stammer D (1997) Atmospheric loading and the oceanic “inverted barometer” effect. *Rev Geophys* 35(1): 79-107. <https://doi.org/10.1029/96RG03037>.

- Wunsch C, Stammer D (1998) Satellite altimetry, the marine geoid, and the oceanic general circulation. *Ann Rev Earth Planet Sci* 26:19-253. <https://doi.org/10.1146/annurev.earth.26.1.219>.
- Wunsch C, Gaposchkin EM (1980) On using satellite altimetry to determine the general circulation of the oceans with application to geoid improvement. *Rev Geophys* 18(4):25-745. <https://doi.org/10.1029/RG018i004p00725>.
- Xu P (1992) A quality investigation of global vertical datum connection. *Geophys J Int* 110(2):361-370. <https://doi.org/10.1111/j.1365-246X.1992.tb00880.x>.
- Zhang L, Li F, Chen W, Zhang C (2009) Height datum unification between Shenzhen and Hong Kong using the solution of the linearized fixed-gravimetric boundary value problem. *J Geod* 83:411-417. <https://doi.org/10.1007/s00190-008-0234-9>.
- Zilkoski DB, Richards JH, Young GM (1992) Results of the general adjustment of the North American Vertical Datum of 1988. *Surv Land Inform Syst* 52:133–149.

–149.